Gutiérrez-Urzúa, L.F., Freddi, F., Di Sarno, L. (2021). Comparative Analysis of Code Based Approaches for the Seismic Assessment of Existing Steel Moment Resisting Frames. Journal of Constructional Steel Research, 181: 106589. https://doi.org/10.1016/j.jcsr.2021.106589

Comparative Analysis of Code-Based Approaches for Seismic Assessment of Existing Steel MRFs

Fernando Gutiérrez-Urzúa[1,*], **Fabio Freddi**[1], **Luigi Di Sarno**[2]

[1]*Dept. of Civil, Environmental & Geomatic Engineering, Univ. College London, London WC1E 6BT, U.K.*

[2] *Dept. of Civil Engineering & Industrial Design, Univ. of Liverpool, Liverpool L69 3BX, U.K.*

[*]Corresponding Author. *E-mail address: f.urzua@ucl.ac.uk*

ABSTRACT

Nowadays, there is a lack of adequate code provisions for the seismic performance and risk assessment of steel structures to be used within European countries. At the same time, in several occasions, existing steel moment resisting frames (MRFs) have demonstrated to be very fragile with respect to seismic actions due to their inadequate ductility capacity. This combination highlights the urgent need for an update of the current Eurocode 8 – Part 3 (EC8-3), thus promoting a reliable assessment of existing steel structures. To this aim, the present study provides a comprehensive and quantitative comparison of the EC8-3 with the three versions of the American ASCE 41 (*i.e.*, ASCE 41-06, -13 and -17), which are here assumed as a reference, as they reflect the evolution of 'similar' assessment procedures during the last two decades. The comparison of the capacity values provided by the codes for different engineering demand parameters (EDPs) highlights significant differences pointing out drawbacks of the EC8-3. In addition, the comparison is made by assessing the seismic performance of two existing steel MRFs, by performing Incremental Dynamic Analyses and deriving fragility curves in a probabilistic approach which considers local EDPs which are compliant with the codes, and that are conventionally used in deterministic studies, *e.g.*, chord rotations in beams and columns, shear strain in panel zones. The comparison of the codes, and the probabilistic assessment of the case studies by using code-based (*i.e.*, local) EDPs, provide significant insights and directions for revision of the EC8-3.

KEYWORDS: Steel moment resisting frames, seismic assessment, existing structures, local engineering demand parameters, incremental dynamic analysis, fragility curves.

1. INTRODUCTION

In the last few decades, earthquake damage in building structures has been documented in Europe and other parts of the world [1–3] and has pushed towards the development of structural design codes including seismic design provisions (*e.g.*, [4,5]). Seismic design codes have been continuously updated with the aim of addressing the structural deficiencies revealed after each strong earthquake, mostly in benefit of the design of new structures. However, many existing structures have been built before the introduction of modern seismic design codes and therefore, are often characterized by deficiencies typical of old design practices [1]. Significant efforts have been made to define procedures and standards for the assessment of the seismic performance of existing structures, however, most of them focused on masonry and reinforced concrete structures, while only a small fraction focused on steel structures (*e.g.*, [6]).

Within this context, the present study provides a comprehensive comparison between code-based assessment provisions for steel moment resisting frames (MRFs), considering all the parameters influencing the definition of the capacity values, such as the seismic demand of the components, modelling parameters and slenderness limits for both European and American steel section profiles. In addition, the comparison is further supported by the assessment of two

case study structures, representative of a low-rise and a mid-rise building. This study relies on a novel probabilistic framework which considers the record-to-record variability while accounting for code-established capacity values, which requires the monitoring of local engineering demand parameters (EDPs) rather than global EDPs. Hence, the present paper allows to identify areas of opportunity for the development of the next generation of the Eurocode 8 – Part 3 (EC8-3) [7] for the seismic assessment of existing steel structures.

Worldwide, steel structures have been extensively used in seismic areas. Their apparently satisfactory seismic performance, along with their architectural and constructional advantages, increased their popularity in the 1960s, 70s and 80s. However, the 1994 Northridge earthquake revealed several deficiencies in the contemporary steel design practices (*e.g.*, lack of capacity design, brittle welding zones, weak panel zones, low-ductility, among others) [1,8]. This confronted the design practices at that time and, as a result, new materials, philosophies and checks were introduced in the design codes [8]. However, these updates mainly focused on the design of new buildings while only a few recommendations were proposed for the retrofitting of existing structures. Regulations for the assessment and retrofitting of existing buildings were a few (*e.g.*, ATC-14 [9]) and often not adequate. For example, most of them aimed at improving the seismic performance of existing structures to reach the safety requirements of newly design buildings, which often resulted in prohibitive associated costs [10], or simply resulted not practical due to the physical constraints of the as-built system. This promoted an extensive effort from the research community in producing more advanced seismic performance and risk assessment procedures.

In the early 1990s, the European Committee for Standardization (CEN) was commissioned with producing the first draft of structural pre-standards to replace the national building regulations from each Member State [11]. This resulted in the publication of the pre-standards for the Eurocodes, including the 1996 Eurocode 8-1-4 [12], which focused on the assessment and retrofit of existing structures. Later, in 2005, the CEN approved and published the EC8-3 [13], which, is the current structural assessment code adopted in most European countries. Although the EC8-3 [13] does not explicitly recognize it, a significant amount of similarities to FEMA 356 [14], suggest that the development of the code was heavily adapted from the latter [7], rather than from its own pre-standard [12]. For example, the EC8-3 [13] defines three qualitative limit states in a performance-based framework, corresponding to different levels of the expected damage, which are qualitatively defined in a similar way to the ones proposed in the FEMA 356 [14]. In addition, several parameters associated with these limit states are shared between these codes, while others are simply adapted to the European regulations' context.

In 2006, the American Society of Civil Engineers (ASCE) released the ASCE 41-06 [15], as an update to FEMA 356 [14], in an attempt to standardize the assessment and rehabilitation practices through the United States. Although this code was intended to establish rehabilitation standards, it heavily relied on implicit off-site assessment procedures. Due to the uncoordinated evolution of the FEMA standards, the ASCE 41-06 contained discrepancies in procedures and philosophies when compared to other ASCE codes [10], such as the ASCE 31-03 [16] and the ASCE 7 [17]. In order to address this issue, the ASCE 41 was updated to its version of 2013 (ASCE 41-13) [18] substituting both the ASCE 31-03 [16] and the ASCE 41-06 [15]. Finally, in 2017, the ASCE released the new version of this standard (ASCE 41-17 [19]), which incorporated significant changes in the hazard calculation, analysis, modeling and acceptance criteria, when compared to its predecessors [15,18]. For steel structures, the most significant changes were related to the modeling and

acceptance criteria definition for steel columns to provide less conservative assessments [19–21], as the ASCE 41-17 [19] relies upon values established from regressions made on experimentally-obtained data available in the literature, which represented a step forward from the values based on simple mechanical relationships used by the ASCE 41-06 [15] and -13 [18].

While the advancements obtained in recent research have been constantly reflected in the ASCE 41 codes with newer versions about every 5 years (*e.g.*, 41-06 [15], -13 [18], -17 [19]), the EC8-3 is still in its version of 2005, which highlights the urgent need for its update to incorporate the current state-of-the-art research. For steel MRFs, several open issues of the current version of the EC8-3 [13] have been highlighted by previous studies and based on the comparison with the 'equivalent' American codes. First, the EC8-3 [13] does not establish modeling parameters and plastic rotation capacity limits that account for simultaneous effects. This issue, as pointed out by Araújo and Castro [22], may lead to the overestimation of the capacity of structural elements. Moreover, Araújo and Castro [7] compared the EC8-3 [13] and the ASCE 41-13 [18] while investigating the seismic response of two case study steel buildings. The outcomes of this study highlighted some of the limitations of the EC8-3 plastic rotation capacity limits and, among others, they suggested that these limits may be inadequate considering that they were simply adapted from the American codes, and therefore, the new versions of the EC8-3 may require tailored provisions based on the European context.

Future versions of the EC8-3 could benefit from the research done on European steel sections in the last few years. For this matter, some researchers have gathered the results of experimental work done on European profiles (*e.g.*, [23,24]) and have developed parametric analyses to fill the gaps in-between the available experimental data. For example, Araújo *et al.* [25] replicated the experiments performed by D'Aniello *et al.* [24] by developing detailed finite element (FE) models, to carry out a parametric study for assessing the influence of global and local geometrical imperfections, the axial load level and the type of loading on the deformation capacity of steel members. The outcomes of this work highlighted that the code systematically overestimates the deformation capacity of deep and slender web cross section profiles. This overestimation is even more pronounced when considering axial loads. In addition, a set of prediction equations for the definition of rotation capacity limits and numerical modeling of steel beam-column members was proposed. More recently, Lignos and Hartloper [26] gathered experimental information on the rotation capacity of European steel shapes and numerically investigated the stability of steel columns and its implications in the seismic assessment of structures within the EC8-3 [13]. They concluded that the current Eurocode provisions for steel columns do not necessarily reflect the column behavioral trends from experimental databases performed on European steel sections. In addition, they proposed steel column modeling parameters (*i.e.*, prediction parameters) based on statistical approaches on column stability experiments and refined models. Other authors have opted for performing building-level parametric analyses to develop simplified methods to relate the building structural properties with a given seismic capacity. Montuori *et al.* [27], for example, proposed a method to evaluate the seismic performance of MRFs by directly comparing simplified pushover-based trilinear capacity curves with demands in an Acceleration-Displacement Response Spectrum (ADRS). The different limit states on the capacity curve were calibrated based on an extensive parametric analysis made on 420 European-profile-based steel MRFs, which were representative of different failure mechanisms (*e.g.*, global mechanism, soft-story mechanism). The outcomes of these studies highlight the need for significant efforts toward the definition of more adequate provisions for the assessment of existing steel structures that can accurately describe the performance of structural elements within European countries.

One of the most significant deficiencies of the current version of the EC8-3 [13] is the lack of modeling parameters and capacity limits for panel zones. The importance of the panel zone behavior in the structural response has been acknowledged by multiple authors since decades ago. Krawinkler and Mohasseb [28], for example, highlighted the importance of including panel zones in the analysis of steel MRFs and used the 'scissors' modeling approach to represent them. Later, Gupta and Krawinkler [29] presented a more refined model for the assessment of American archetype structures within the SAC project. As highlighted by the authors, the inclusion of panel zones in the modeling of a steel MRF may influence the performance of the structure in post-Northridge structures (*i.e.,* capacity design considered), moreover, it will likely control the performance in pre-Northridge structures, as confirmed later in this paper. Although the inclusion of panel zones has become common in the non-linear analysis of steel MRFs, the EC8-3 [13] did not incorporate modeling parameters or capacity limits for these elements. Di Sarno and Wu [6] overcame this limitation by using the modeling approach proposed by Gupta and Krawinkler [29], and the capacity limits established by the American codes, in the assessment of an infilled steel MRF located in Amatrice (Italy), which was damaged during the 2016 Central Italy earthquakes. The authors investigated several non-linear modeling strategies, with and without considering the deformability of the panel zones. The outcomes highlighted that the presence of the panel zones significantly affect the behavior of the structure and that, for the case study investigated, the capacity of the bare frame structure was controlled by the deformation in panel zones.

Although the deformation of a structure is controlled by its components (*e.g.*, columns, panel zones, connections, beams), in seismic risk assessment procedures, it is a common practice to measure the structural damage by using simpler global EDPs. Global EDPs, such as the inter-story drift ratio (IDR), are often proposed in assessment guidelines (*e.g.*, [14,15]) and used in multiple research studies (*e.g.*, [30–32]) to synthetically describe the seismic response and indirectly monitor the demand imposed on the components. However, due to the lack of modern seismic design rules in existing buildings, such as strength hierarchy (*i.e.,* capacity design), global EDPs may not be representative of the local seismic demand [33], as (1) the capacity may be governed by force-controlled actions, (2) the local capacity of the multiple elements along the story level is not necessarily uniform, and (3) the story drift may be enabled by combined local demand mechanisms (*e.g.*, rotation in beams plus panel zone strain, instead of a large rotation in beams). Therefore, the establishment of capacity limits based on a uniform value of IDR may not be adequate to reflect the damage in the structural elements [33].

To overcome this limitation, only few research studies have investigated the seismic performance of existing structures in probabilistic risk assessment frameworks by considering local EDPs. Among others, Freddi *et al.* [33] performed Incremental Dynamic Analyses (IDA) [34] to evaluate the fragilities for both the system and the components of a reinforced concrete frame retrofitted with buckling restrained braces. The outcomes show how the use of global EDPs may be inadequate in some situations. Similarly, Freddi *et al.* [35] investigated the definition of Probabilistic Seismic Demand Models for local EDPs while performing Cloud Analyses on a reinforced concrete frame. The authors concluded that the use of a probabilistic component-based approach (*i.e.*, using local EDPs) provides a more comprehensive understanding of the structural behavior of the analyzed building. Song *et al.* [36] recently performed a probabilistic assessment of the seismic demands and fracture capacity of welded column splice connections, *i.e.*, local EDP, in steel

MRFs. The study was based on Cloud and Monte Carlo analyses and focused on two case study structures providing insights on the influence of relevant uncertainties on the assessment of fracture fragility of welded column splices.

The quantification of uncertainties is essential in the seismic risk assessment of structures. In this context, EDPs play a crucial role, as they are used as a measure of structural and non-structural damage to be correlated with decision variables, such as repairing cost and downtime [35,37]. Previous studies have demonstrated that the effects of epistemic uncertainty (material properties, geometry) is generally less notable than the effects of the aleatory uncertainty (record-to-record variability) [38,39]. Hence, the present study neglects the variability related to the uncertainty in materials and geometric properties and account only for the uncertainty related to the seismic input for the assessment of the two case study structures. To account for the record-to-record variability in the seismic vulnerability assessment of structural systems, a popular approach involves the development of fragility curves (*e.g.*, [30–33]). These tools provide the probability of exceeding a specified limit state or a defined failure condition for different levels of seismic intensity, measured by using an appropriate Intensity Measure (IM) (*e.g.*, [35,40]). Several studies investigated the seismic performance of existing structures by accounting for the uncertainties related to the seismic input by using fragility curves, including studies with steel buildings. For example, Molina Hutt *et al.*[30] investigated the vulnerability of steel MRF built in the 1970s, by using the conditional spectrum method. In a similar way, Kazantzi *et al.* [31] studied the performance of a 3 story pre-Northridge case study building, designed for the SAC project [29] and located in Los Angeles. They used fragility curves developed through a Monte Carlo simulation, to account for the uncertainty attained to the ground motion variability. Likewise, Kia and Banazadeh [32] developed fragility curves for IDRs related to different levels of damage in regular multi-story steel buildings, accounting for the record-to-record variability and other sources of uncertainty by using a Bayesian regression inference. It is worth mentioning that in these studies, only global EDPs (*i.e.*, IDR) have been considered.

The present paper compares the outcomes of assessment procedures performed by using capacity limits for component level EDPs (*i.e.*, local EDPs) established by European and American codes, in order to provide preliminary insights for the revision of the EC8-3. First, a few considerations are made among all the codes to identify common aspects in order to reduce the number of variables to be investigated. Then, a side-by-side comparison of the capacity limits between the EC8-3 [13] and the different versions of the ASCE 41 [15,18,19] is made, considering the discrepancies in the available yield capacity values offered by the codes, including the definition of demand-dependent capacity values. The comparison is made with the above-mentioned American codes as they represent the state-of-the-art in the code-based assessment procedures. A parametric analysis is carried out on catalogue-based steel shapes to establish an equivalency between the European and American slenderness terms and draw a comparison in terms of capacity limits. Finally, the assessment procedures outlined by the codes are used on two low-code steel MRFs selected as case study structures (*e.g.*, [29]) to be used as test-bed for the comparison of the codes. The assessment is performed based on three local EDPs as implemented in the considered codes, *i.e.*, column's chord rotation, beam's chord rotation and panel zone's shear strain, while global EDPs are simultaneously monitored for contextual purposes. IDAs [34] are performed for the development of components and system level fragility curves, which allow the comparison of capacity limits established on each code accounting for the uncertainty related to the seismic input and considering the variation in the seismic demands related to the ground motion time-history.

2. ALIGNMENT OF THE CODES

This section presents a contextual comparison of some aspects in the EC8-3 [13] and the ASCE 41 [15,18,19], in order to establish a shared starting point for the consistent comparison of the capacity values of the local EDPs which is discussed in the following section. Even though the two most recent versions of ASCE 41 [18,19] contain three assessment approaches, only Tier 3 is considered in this paper, as it is the only approach comparable with the procedures contained in the EC8-3 [13] and the ASCE 41-06 [15]. Figure 1 shows a flow chart representing the main steps that are conventionally involved in the non-linear assessment procedures for individual structures, when following the approaches used in this paper.

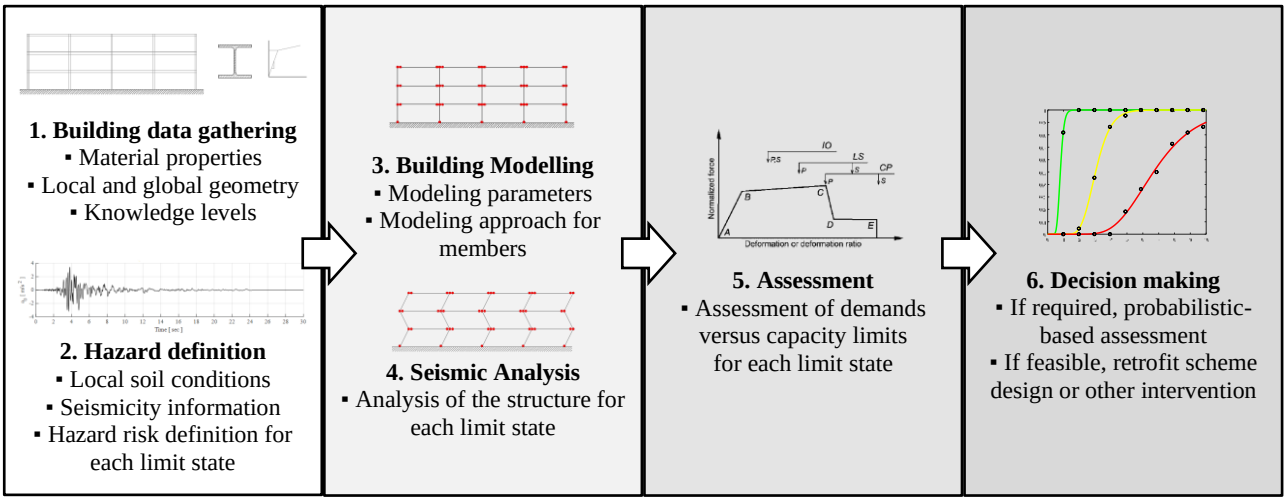

Figure 1. Steps conventionally involved in the seismic performance non-linear assessment procedures.

2.1 Knowledge levels

Epistemic uncertainties (*e.g.*, lack of information on geometry, material properties, detailing, etc.) affect the assessment of existing structures [38,39,41]. The EC8-3 [13] addresses this issue by considering knowledge levels (KL) and confidence factors (CF_{KLn}). The knowledge levels establish different minimum knowledge thresholds, while the confidence factors reduce the capacity of the structural components to penalize poor knowledge levels. Knowledge levels depend on material testing, availability of drawings, visual assessment, etc. and hence, this approach encourages the practitioner to gather additional and detailed information on the structure to reduce the conservativism of the assessment. The EC8-3 [13] specifies three knowledge levels, being KL1 (limited knowledge) the lowest, KL2 (normal knowledge) the intermediate, and KL3 (full knowledge) the highest. The first knowledge level, KL1 is characterized by limited in-situ inspection and limited material testing, with a structural analysis based only on the standards at the time of construction and relevant practice. This knowledge level only allows the use of linear procedures (*i.e.*, increasing the conservativeness of the analysis), while requires the reduction of the capacity of structural elements by a confidence factor of $CF_{KL1} = 1.35$ (*i.e.*, dividing the capacity by 1.35), to account for the epistemic uncertainty related to a poor building knowledge. The second knowledge level, KL2, is characterized by an extended in-situ inspection and material testing, or a combination of detailed original construction specifications and limited in-situ inspection and testing. The KL2 allows the use of non-linear procedures and reduces the capacity of structural elements only by $CF_{KL2} = 1.2$. Finally, the full knowledge level, KL3, requires either a comprehensive in-situ inspection and material testing, or a combination of detailed original construction specifications, drawings and reports, with a limited in-situ inspection and material testing.

Similarly, KL3 allows the use of non-linear procedures, but does not reduce the capacity of structural elements, *i.e.*, CF_{KL3} = 1.0.

In a similar way, the several versions of ASCE 41 [15,18,19] establish knowledge factors (κ) from 0.75 to 1.00, which multiply the material capacities, depending on the level of knowledge. Similarly to EC8-3 [13], the lowest levels of knowledge only allow linear analysis procedures. For the purpose of this paper, full knowledge of the structure is assumed in all cases, therefore, both the CF_{KLn} and κ are considered to be equal to 1.

2.2 Limit states

Limit states are used to define boundaries between continuous damage states (DSs). They define qualitative thresholds based on structural or non-structural observations which reflect the overall state of the structure and, simultaneously, can be related to measurable capacity limits (or acceptance criteria, as defined in the American codes) for each EDP (*e.g.*, stress, strain, chord rotation, inter-story drifts, energy dissipation).

The EC8-3 [13] defines three limit states, which describe the structural and the non-structural damage on the building simultaneously. On the other hand, the American codes [15,18,19] untie the structural and non-structural damage and define three structural performance levels (*i.e.*, structural limit states) and five non-structural performance levels (*i.e.*, non-structural limit states). The present paper focuses on the structural performance only while the assessment of the performance of non-structural components is beyond the scope of the present study.

Although the three limit states in the EC8-3 [13] and the corresponding structural performance levels in the ASCE 41 [15,18,19] are not exactly defined in the same way for all codes, in this study, they are considered equivalent as they are all based on the definitions established by FEMA 356 [14], as pointed out by Fardis [11]. The three limit states can be broadly classified as: (1) Limit State 1 (LS1), which is correlated to a structure with only slight damage, in which the structural elements retain the pre-earthquake strength and stiffness; (2) Limit State 2 (LS2), which is associated to a damaged structure that shows some permanent drift, but retains some residual strength and stiffness and is capable of withstanding some lateral loads (*e.g.*, moderate aftershocks); and (3) Limit State 3 (LS3), which is correlated to a near collapse building, damaged beyond repair, with large permanent drift and little residual strength and stiffness. Table 1 shows the described limit states as defined in the codes [13,15,18,19].

Table 1. Assumed equivalency of limit states among different codes.

Code	Limit State 1 (LS1)	Limit State 2 (LS2)	Limit State 3 (LS3)
EC8-3 [13]	Damage Limitation	Significant Damage	Near Collapse
ASCE-41 [15,18,19]	Immediate Occupancy	Life Safety	Collapse Prevention

2.3 Hazard levels

In a performance-based assessment framework, different levels of seismic performance (*e.g.*, limit states) are correlated to different levels of seismic hazard. The definition of the hazard level plays a major role in the seismic assessment of a structure. However, in the present paper the comparison of the assessment procedures focuses on the different definition of the capacity limits, for different EDPs, and for the different seismic codes by considering an approach that makes the

evaluation independent from the seismic hazard. Nonetheless, to provide a comprehensive overview of the assessment procedures, a brief description of key aspects related to the seismic hazard definition are reported in the following.

The EC8-3 [13], suggests that for building structures the following hazard levels should be used: a return period of 225 years (20% probability of exceedance in 50 years) for LS1; 475 years (10% probability of exceedance in 50 years) for LS2; and 2,475 years (2% probability of exceedance in 50 years) for LS3, which are further modified by importance factors (from 0.9 to 1.4) and in some cases, by the country's National Annex [4].

On the other hand, in the American codes [15,18,19] the different levels of seismic performance are correlated to different levels of seismic hazard by a matrix. In this case, differently from the EC8-3, the stakeholders (*e.g.*, owner, authorities) are in charge of deciding what performance level should be linked to each hazard level. However, the codes provide suggestions of this correlation based on the risk category of the structures defined according to the ASCE 7-16 [5]. For example, for an existing structure in the risk category II (*e.g.*, a small office building), the Basic Performance Objective for Existing Buildings (BPOE) suggest return periods of 225 years for LS1, and 975 years for LS3.

3. CODE-BASED CAPACITY VALUES IN STEEL MOMENT RESISTING FRAMES

Three code-based component-level EDPs are considered in this study: (1) chord rotation in columns; (2) chord rotation in beams; (3) shear strain in panel zones. These EDPs relate to the main damage patterns within steel MRFs and are those conventionally considered by assessment codes. In the present study, beam-to-column connections are considered fully rigid, with no failure occurrence, therefore, the capacity parameters and values for these components are not discussed. In addition, some of the most common global EDPs used in literature are discussed.

3.1 Code-based yield capacity parameters

The assessment of ductile components in steel MRFs is conventionally based on the definition of deformation-based yield capacity parameters which, for beams and columns, is represented by the chord rotation at yielding (θ_y), and for panel zones, is represented by the shear yield strain (γ_y).

In the EC8-3 [13], the capacity limits for beams and columns are given in terms of θ_y, however the EC8-3 does not provide indications on this parameter and the following analytical relationship is assumed:

$$\theta_y = \frac{M_{pb,Rd} L}{6EI} \quad (1)$$

where $M_{pb,Rd}$ is the plastic moment capacity of the element at the location of the plastic hinge; L is the length of the span or height of the story (*i.e.*, length of the beam or height of the column); and EI are the Young's modulus and moment of inertia of the element, respectively. It is worth mentioning that the formulation of Eq. 1 assumes an antisymmetric deformation along the beam (*i.e.*, shear length equal to half of the beam) and does not consider the influence of the axial load on the rotation capacity of the element.

The ASCE 41-06 and -13 [15,18] explicitly provide the parameters to build the complete moment-rotation relationship for beams and columns, including rotation and moment values at yield. For beams, these codes use the same relationship as in Eq. 1. Conversely, for columns, Eq. 1 is modified to account for the axial load, as follows:

$$\theta_y = \frac{M_{pb,Rd}L}{6EI}(1-\nu) \quad (2)$$

where ν is the dimensionless axial force and is defined as $\nu = N_k/N_{pl,Rd}$. N_k is the total axial force demand (*i.e.*, gravity plus seismic overturning effects) and $N_{pl,Rd}$ is the axial capacity of the cross section.

The ASCE 41-17 [19] further improve the formulations for θ_y by accounting for the shear stiffness of the element. For beams, Eq. 1 is modified as follows:

$$\theta_y = \frac{M_{pb,Rd}L}{6EI}\left(1+\frac{12EI}{L^2GA_s}\right) \quad (3)$$

where G is the shear modulus of steel and A_s is the effective shear area of the cross section in a wide-flange beam. For columns, in addition of accounting for the shear stiffness of the element, the ASCE 41-17 [19] simplifies the formulation considering only the axial force due to the gravity loads and discards the overturning effects, as follows:

$$\theta_y = \begin{cases} \text{for } \nu_G < 0.2 & \frac{M_{pb,Rd}L}{6EI}\left(1+\frac{12EI}{L^2GA_s}\right)\left(1-\frac{\nu_G}{2}\right) \\ \text{for } 0.2 \le \nu_G \le 0.5 & \frac{M_{pb,Rd}L}{6EI}\left(1+\frac{12EI}{L^2GA_s}\right)\left(\frac{9}{8}-\frac{9\nu_G}{8}\right) \\ \text{for } 0.5 < \nu_G & \frac{M_{pb,Rd}L}{24E\nu_G(1-\nu_G)I}\left(1+\frac{12EI}{L^2GA_s}\right)\left(\frac{9}{8}-\frac{9\nu_G}{8}\right) \end{cases} \quad (4)$$

where ν_G is the dimensionless gravity axial force and is defined as $\nu_G = N_G/N_{pl,Rd}$ where N_G is the axial force demand related to the gravity loads. This approach simplifies the rotation capacity calculation by establishing a fixed value through the analysis, *e.g.*, in time-history analyses the rotation capacity is constant at each step of the ground motion. If compared with the ASCE 41-06 and -13 [15,18], the different formulation of ASCE 41-17 [19] together with the considerations for the shear stiffness and for ν_G instead of ν, results in an overall increase of the θ_y for both beams and columns, which, according to Lignos *et al.* [42] and Pekelnicky [20], results in less conservative assessments.

Deformation-based capacity values for panel zones are provided only by the ASCE 41-17 [19] in terms of yield shear strain, as indicated in Eq. 5:

$$\gamma_y = \frac{f_{ye}}{G\sqrt{3}}\sqrt{1-\nu_G{}^2} \quad (5)$$

where f_{ye} is the expected yield strength of the panel zone. A summary of the deformation-based yield capacity parameters for the different components is reported in Table 2.

Table 2. Deformation-based capacity parameters for each EDP for the analyzed codes.

Code	Beams θ_y	Columns θ_y	Panel zones γ_y
EC8-3 [13]	Not given, assumed Eq. 1	Not given, assumed Eq. 1	Not given
ASCE 41-06 [15]	Eq. 1	Eq. 2	Not given
ASCE 41-13 [18]	Eq. 1	Eq. 2	Not given
ASCE 41-17 [19]	Eq. 3	Eq. 4	Eq. 5

3.2 Code-based capacity limits

Capacity limits (acceptance criteria in the American codes) are defined for each limit state and EDP. It is worth to mention that only the primary elements are considered in the present study.

3.2.1 Beams

For beams, all considered codes provide capacity limits, in terms of plastic rotation thresholds, based on the slenderness characteristics of web and flanges where the least favorable rules the classification of the whole section. The EC8-3 [13] classifies the sections based on the recommendations of the Eurocode 3 Part 1-1 (EC3-1-1) [43] and provides different plastic rotation capacity limits for sections 'Class 1' and 'Class 2'. Sections 'Class 3' and 'Class 4' are treated as force-controlled elements, although, this may underestimate the plastic rotation capacity of sections 'Class 3', as commented by Lignos and Hartloper [26]. In a similar way, the American codes [15,18,19] determine two sets of plastic rotation capacity limits based on the local slenderness ratios, moreover, they also define a continuous interpolation region for those sections with characteristics that fall between the two limits.

The plastic rotation capacity limits for beams, are reported in Table 3 as a function of the parameters identifying the slenderness limits for the web (*i.e.,* α_E and α_A) and for the flanges (*i.e.,* β_E and β_A), and hence the Class, of the sections. Eq. 6 shows the slenderness parameters for the EC8-3 [13], while Eq. 7 shows them for the ASCE 41 codes [15,18,19]. It is worth mentioning that Eqs. 6 and 7 have been derived by rearranging the equations from both codes for uniformity purposes through this paper and in order to simplify the comparison:

$$\alpha_E = \frac{d}{t_w}\sqrt{f_{ye}} \qquad \beta_E = \frac{c}{t_f}\sqrt{f_{ye}} \tag{6}$$

$$\alpha_A = \frac{h_i}{t_w}\sqrt{f_{ye}} \qquad \beta_A = \frac{b_f}{2t_f}\sqrt{f_{ye}} \tag{7}$$

where d, c, h_i, b_f, t_w and t_f are parameters related to the dimensions of the steel shape as shown in Figure 2. For the above formulas, f_{ye} should be expressed in MPa, to ensure compatibility with the slenderness limits shown later in this paper.

The most conservative slenderness limits (*e.g.,* those that define the 'Class 1' sections for the EC8-3) are similar for all codes as they have all evolved from the FEMA 356 [14]. However, the different definition of the flange and web slenderness parameters (*i.e.,* α and β), affects the direct comparison between codes. For the most compact sections (*e.g.,* 'Class 1'), the plastic rotation capacity limits in the EC8-3 are the same as in the ASCE 41-06, which is a result of both codes being based on FEMA 356 [14]. In the newer versions of ASCE 41 [18,19] these values tend to be less conservative. For sections 'Class 2', the EC8-3 [13] establishes plastic rotation capacity limits which are equal to those given for the least ductile sections defined by the American codes.

The plastic rotation capacity limit can be compared in terms of θ_y for all codes, however, it should be noted that θ_y is calculated differently for the ASCE 41-17 [19] (see Eq. 3), therefore, the actual plastic rotation capacity limits will vary even when the limits on Table 3 are shown to be the same.

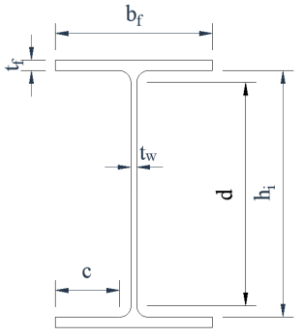

Figure 2. Steel cross section parameters.

Table 3. Slenderness limits for the classification of beams and plastic rotation capacity limits.

Code	Slenderness limits	Plastic rotation capacity limits		
		LS1	**LS2**	**LS3**
EC8-3 [13] [1]	$\alpha_E \leq 1104$ and $\beta_E \leq 138$ (Class 1)	1.0 θ_y	6.0 θ_y	8.0 θ_y
	$\alpha_E \leq 1272$ and $\beta_E \leq 153$ (Class 2)	0.25 θ_y	2.0 θ_y	3.0 θ_y
	$\alpha_E > 1272$ or $\beta_E > 153$ (Class 3 or 4)	Force-controlled		
ASCE 41-06 [15] [2]	$\alpha_A \leq 1098$ and $\beta_A \leq 137$	1.0 θ_y	6.0 θ_y	8.0 θ_y
	Other intermediate values	Interpolate		
	$\alpha_A \geq 1682$ or $\beta_A \geq 171$	0.25 θ_y	2.0 θ_y	3.0 θ_y
ASCE 41-13 [18] [2]	$\alpha_A \leq 1098$ and $\beta_A \leq 137$	1.0 θ_y	9.0 θ_y	11.0 θ_y
	Other intermediate values	Interpolate		
	$\alpha_A \geq 1682$ or $\beta_A \geq 171$	0.25 θ_y	3.0 θ_y	4.0 θ_y
ASCE 41-17 [19] [2,3]	$\alpha_A \leq 1123$ and $\beta_A \leq 137$	2.25 θ_y	9.0 θ_y	11.0 θ_y
	Other intermediate values	Interpolate		
	$\alpha_A \geq 1723$ or $\beta_A \geq 174$	1.0 θ_y	3.0 θ_y	4.0 θ_y

[1] Sections that comply with both 'Class 1' and 'Class 2' criteria must be classified as 'Class 1'.

[2] Interpolation must be made for web and flange slenderness limits. The lower plastic rotation limit should be taken for each limit state.

[3] Slenderness limits in ASCE 41-17 [19] are function of E which is assumed as 210 GPa to allow the direct comparison on the codes.

As the definition of the slenderness parameters is different for the European and the American codes in Table 3, the comparison between slenderness limits in the codes has to be done on a case by case basis. Figure 3, shows the relationship between the slenderness parameters as defined in Eqs. 6 and 7, considering both European (IPE and HE) and American steel sections (W sections). European profiles tend to have slightly higher α_A to α_E and β_A to β_E ratios when compared to American ones, which reflects a generally larger relative size of the web-to-flange fillet in the European shapes. However, the full IPE, HE and W steel shape catalogues were used for the fitting of a linear relationship between the slenderness parameters to allow a general comparison between codes.

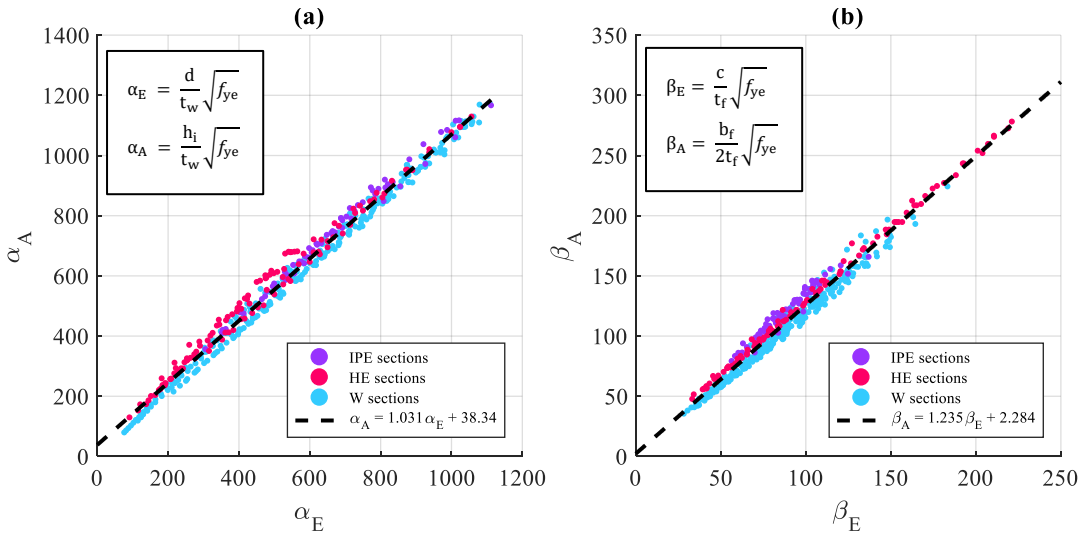

Figure 3. Relationship of slenderness parameters between the EC3-1-1 [43] and the ASCE 41 [15,18,19], for European IPE and HE, and American W steel sections: (a) relationship between α_E and α_A; (b) relationship between β_E and β_A.

Figure 4 illustrates the comparison of the plastic rotation capacity limits between the codes. In order to allow the comparison of entire steel section catalogues, rather than individual shapes, the slenderness parameters for the ASCE 41 codes [15,18,19] (α_A and β_A) were transformed into α_E and β_E terms, by using the regression from Figure 3. As it can be observed, the EC8-3 [13] provides less conservative capacity limits for all limit states, at most values of α_E. Most of the catalogue sections shown in Figure 3 exhibit values of $\alpha_E < 1100$, for steel A572, therefore, would be catalogued as web 'Class 1'. On the other hand, depending on the value of the slenderness parameter β_E, the capacity values may be more or less conservative in the EC8-3 [13] than in the ASCE 41 [15,18,19]. As Figure 4 is given in terms of θ_y, the actual capacity values for the ASCE 41-17 may not be directly comparable with the rest of the codes, as the definition of θ_y differs.

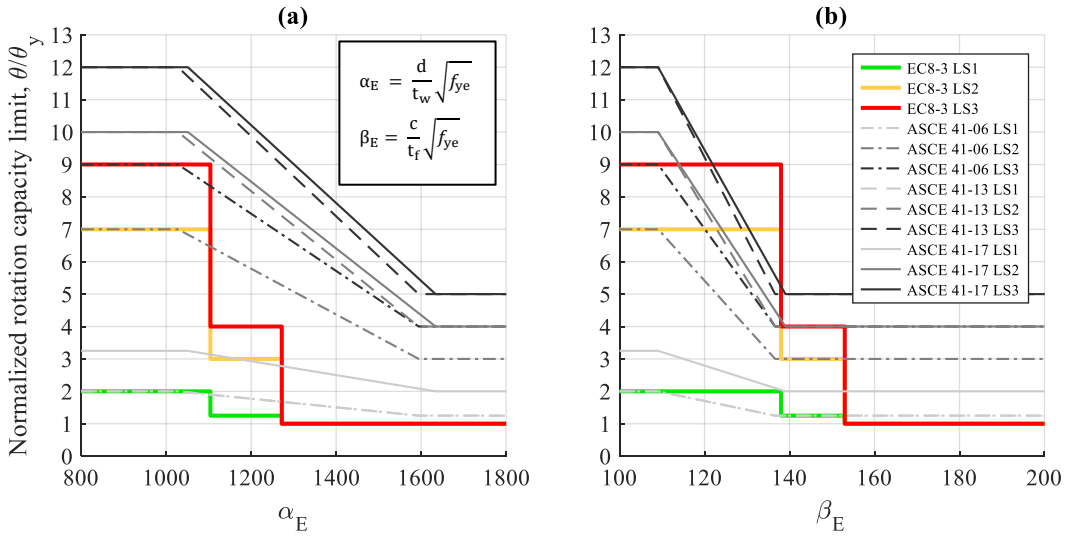

Figure 4. Normalized rotation capacity limits (θ/θ_y) for beams vs. slenderness parameters. For (a) web slenderness, α_E and (b) flange slenderness, β_E. f_{ye} assumed as 1.1×345 MPa (steel A572).

3.2.2 Columns

The capacity limits for the plastic rotation of the columns are defined similarly to the beams, with the inclusion of the additional parameter accounting for the influence of the axial load. A summary of the plastic rotation capacity limits for columns is given in Table 4. Similar to the beams, the slenderness limits formulation has been rearranged for uniformity purposes and E is assumed as 210 GPa.

In the EC8-3 [13], columns with a dimensionless axial force $\nu < 0.3$, are treated in a similar way to beams. The only exception is related to the slenderness limits established for the column web, as it now is expected to work mostly in compression. All columns with $\nu \geq 0.3$ must be treated as force-controlled elements.

According to the ASCE 41-06 [15] and -13 [18], columns are considered as deformation-based components for $\nu < 0.5$. In these codes, the section classification and some of the plastic rotation capacity limits are function of the dimensionless axial force ν as well. In addition, it is important to stress out that, for these codes, the definition of the chord yielding rotation θ_y for columns is also function of the dimensionless axial force ν, as observed in Eq. 2.

In the ASCE 41-17 [19], the plastic rotation capacity limits are decoupled from θ_y and they are defined in terms of the ductility parameters a and b, both defined in Eqs. 8 and 9:

$$a = \begin{cases} 0.8(1-\nu_G)^{2.2}\left(0.1\frac{L}{i_z}+0.8\frac{h_i}{t_w}\right)^{-1} - 0.0035 \geq 0 & (8a) \\ 1.2(1-\nu_G)^{1.2}\left(1.4\frac{L}{i_z}+0.1\frac{h_i}{t_w}+0.9\frac{b}{t_f}\right)^{-1} - 0.0023 \geq 0 & (8b) \end{cases}$$

$$b = \begin{cases} 7.4(1-\nu_G)^{2.3}\left(0.5\frac{L}{i_z}+2.9\frac{h_i}{t_w}\right)^{-1} - 0.006 \geq 0 & (9a) \\ 2.5(1-\nu_G)^{1.8}\left(0.1\frac{L}{i_z}+0.2\frac{h_i}{t_w}+2.7\frac{b}{t_f}\right)^{-1} - 0.0097 \geq 0 & (9b) \end{cases}$$

where i_z is the radius of gyration on the weak axis. The parameter a is used to represent the plastic rotation between the yielding point and the point at which the load capacity drops to its residual value, whereas, parameter b represents the plastic rotation between the yielding point and the point at which the residual capacity is reduced to zero (*i.e.*, rupture). The use of Eqs. 8a and 9a, or Eqs. 8b and 9b, depends on the dimensionless gravity axial force ν_G and the slenderness parameters α_A and β_A, as summarized in Table 5.

The relationship between ν (or ν_G) and the total rotation capacity limits for four cross sections presented in Table 6, is shown in Figure 5. The comparison has been made directly in the cross sections to understand the effects of axial force on the deformation capacity limits established by the different codes. The considered sections have been extracted from the two case study structures analyzed in the following section, and which characteristics fit as below, above and in-between the slenderness limits established by the ASCE 41 [15,18,19], as detailed in Table 6. For each code and limit state, the characteristics of the rotation limit are affected by: (1) the different definition of slenderness limits; (2) the differences in the definition of θ_y; and (3) the different definition of the dimensionless axial force. It is not possible to directly compare the ASCE 41-17 [19], as only gravity loads are considered, except in the case in which $\nu_G = \nu$ (*i.e.*, columns in which the overturning effects are negligible).

Figure 5 shows four cross sections that are classified as different classes according to the EC3-1-1 [43]. Figure 5(a), (b), and (c) show respectively the curves for sections W14×283, W14×99 and W14×74 which are classified as 'Class 1' and 'Class 2' according to the EC8-3 [13] and hence, allow the development of plastic rotation for $\nu \leq 0.3$. On the other hand, for section W14×61 shown in Figure 5(d), the development of plastic rotation is not allowed at any point, as it is classified as 'Class 3'. The vertical axes in Figure 5 show the total rotation rather than the plastic rotation, to allow a direct comparison of θ_y definition in-between codes.

Table 4. Slenderness limits for the classification of columns and plastic rotation capacity limits.

Code	Dimensionless axial load limits	Slenderness limits [2]	Plastic rotation capacity limits		
			LS1	LS2	LS3
EC8-3 [13] [1]	$\nu < 0.3$	$\alpha_E \leq 506$ and $\beta_E \leq 138$ (Class 1)	1.0 θ_y	6.0 θ_y	8.0 θ_y
		$\alpha_E \leq 583$ and $\beta_E \leq 153$ (Class 2)	0.25 θ_y	2.0 θ_y	3.0 θ_y
		$\alpha_E > 583$ or $\beta_E > 153$ (Class 3 or 4)		Force-controlled	
	$0.3 \leq \nu$	All		Force-controlled	
ASCE 41-06 [15] [2]	$\nu < 0.2$	$\alpha_A \leq 788$ and $\beta_A \leq 137$	1.0 θ_y	6.0 θ_y	8.0 θ_y
		Other intermediate values		Interpolation	
		$\alpha_A \geq 1209$ or $\beta_A \geq 171$	0.25 θ_y	2.0 θ_y	3.0 θ_y
	$0.2 \leq \nu \leq 0.5$	$\alpha_A \leq 1098$ and $\beta_A \leq 137$	0.25 θ_y	8 (1-5ν/3) θ_y	11 (1-5ν/3) θ_y
		Other intermediate values		Interpolation	
		$\alpha_A \geq 1682$ or $\beta_A \geq 171$	0.25 θ_y	0.5 θ_y	0.8 θ_y
	$0.5 < \nu$	All		Force-controlled	
ASCE 41-13 [18] [2]	$\nu < 0.2$	$\alpha_A \leq 788$ and $\beta_A \leq 137$	1.0 θ_y	9.0 θ_y	11.0 θ_y
		Other intermediate values		Interpolation	
		$\alpha_A \geq 1209$ or $\beta_A \geq 171$	0.25 θ_y	3.0 θ_y	4.0 θ_y
	$0.2 \leq \nu \leq 0.5$	$\alpha_A \leq 1098$ and $\beta_A \leq 137$	0.25 θ_y	14 (1-5ν/3) θ_y	17 (1-5ν/3) θ_y
		Other intermediate values		Interpolation	
		$\alpha_A \geq 1682$ or $\beta_A \geq 171$	0.25 θ_y	1.2 θ_y	1.2 θ_y
	$0.5 < \nu$	All		Force-controlled	
ASCE 41-17 [19] [3]	$\nu_G \leq 0.6$	All	0.5 a	0.75 b	b
	$0.6 < \nu_G$	All		Force-controlled	

[1] Sections that comply with both 'Class 1' and 'Class 2' criteria must be classified as 'Class 1'.

[2] Interpolation must be made for web and flange slenderness limits. The lower plastic rotation limit should be taken for each limit state.

[3] The terms 'a' and 'b' are defined as in Eqs. 8 and 9.

The definition of θ_y in the American codes (Eqs. 2 and 4) significantly influences the rotation capacity at the highest values of ν, however, it is negligible in the low axial zone of the curves, as can be observed by comparing the rotation limits in the EC8-3 [13] and the ASCE 41-06 [15]. Considering that the EC8-3 [13] restricts the development of plastic rotation to columns with $\nu < 0.3$, the use of either Eq. 1 or Eq. 2 for the definition of θ_y does not significantly affect the plastic rotation capacity limits. When comparing the ASCE 41-06 [15] with its successors, the ASCE 41-13 [18] reflects less conservative plastic rotation capacity limits, however, the slenderness boundaries and the influence of the dimensionless axial forces (ν) remain the same. With regards to the ASCE 41-17 [19], it can be observed that for the

sections of Figure 5(a) and (b), the plastic rotation capacity limits are less conservative even when assuming that $\nu = \nu_G$. On the other hand, for the other two sections of Figure 5(c) and (d) the plastic rotation capacity limits of the newest version of the ASCE 41 are likely to be more conservative than the ones established by its predecessors.

Table 5. Plastic rotation parameters based on slenderness limits, according to ASCE 41-17 [19].

Dimensionless axial gravity force, ν_G	Slenderness limits [1]	Equations to use
$\nu_G < 0.2$	$\alpha_A \leq 1123(1\text{-}0.71\nu_G)$ and $\beta_A \leq 137$	Eqs. 8a and 9a
	Other intermediate values	Interpolate
	$\alpha_A \geq 1723(1\text{-}1.83\nu_G)$ or $\beta_A \geq 174$	Eqs. 8b and 9b
$0.2 \leq \nu_G \leq 0.6$	$\alpha_A \leq 353(2.93\text{-}\nu_G)$ and $\beta_A \leq 137$	Eqs. 8a and 9a
	Other intermediate values	Interpolate
	$\alpha_A \leq 513(2.33\text{-}\nu_G)$ or $\beta_A \leq 174$	Eqs. 8b and 9b

[1] Interpolation must be made for web and flange slenderness limits. The lower ductility parameters a and b should be taken.

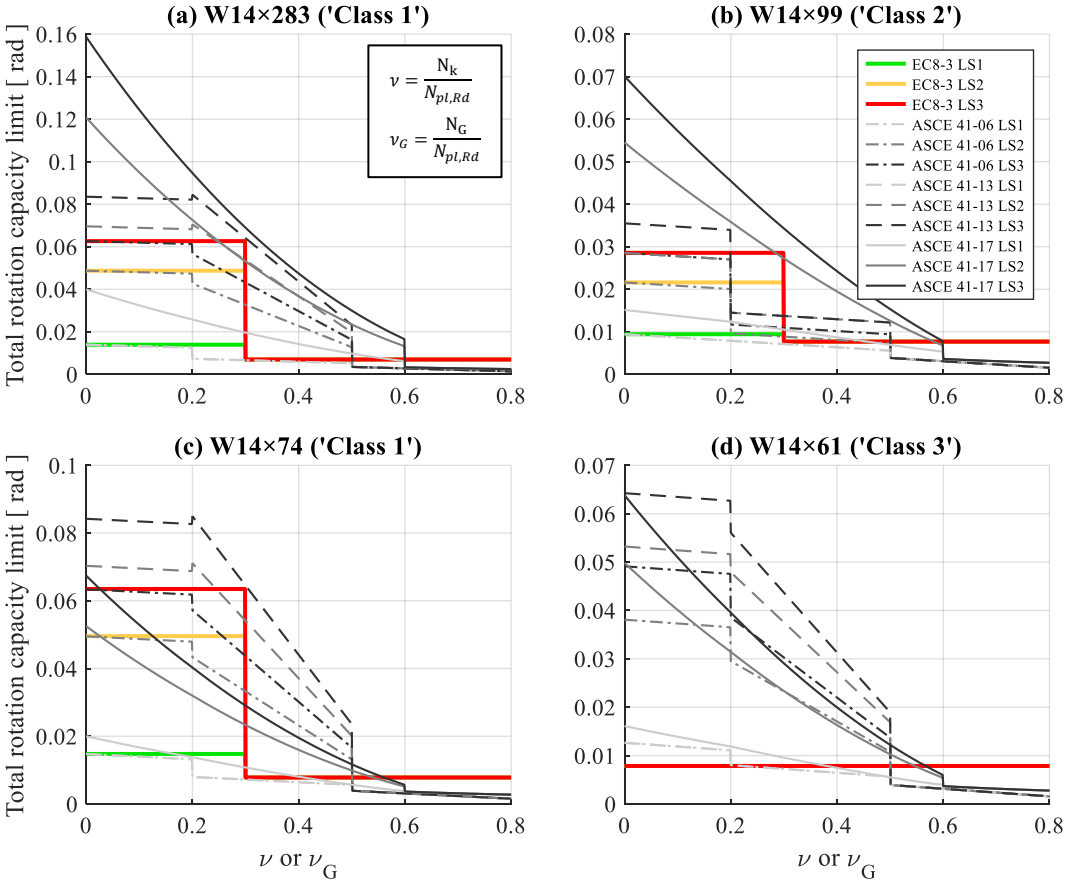

Figure 5. Total rotation capacity limit (elastic plus plastic) (θ) for columns vs. dimensionless axial force ν (or ν_G). Column sections (a) W14×283; (b) W14×99; (c) W14×74; (d) W14×61.

Table 6. Classification of selected sections according to their slenderness.

Code	Slenderness region [1,2]			
	W14×283	**W14×99**	**W14×74**	**W14×61**
EC8-3 [13]	'Class 1'	'Class 2'	'Class 1'	'Class 3'
	$\alpha_E = 164$	$\alpha_E = 424$	$\alpha_E = 489$	**$\alpha_E = 585$**
	$\beta_E = 62$	**$\beta_E = 150$**	$\beta_E = 103$	$\beta_E = 125$
ASCE 41 [15,18,19]	Below lower limit	Above higher limit	Below lower limit	Interpolation region
	$\alpha_A = 190$	$\alpha_A = 508$	$\alpha_A = 547$	$\alpha_A = 655$
	$\beta_A = 76$	**$\beta_A = 182$**	$\beta_A = 125$	**$\beta_A = 151$**

[1] Slenderness parameters calculated with $f_{ye} = 1.1 \times 345$ MPa (steel A572).

[2] Bold values are those ruling the slenderness classification.

3.2.3 Panel Zones

For panel zones, the American codes [15,18,19] provide guidelines for the determination of the deformation capacity limits for the panel zones, either in terms of yield shear strain (γ_y) or equivalent yield rotation (θ_y), as they are analogous. The EC8-3 [13] lacks of explicit capacity limits for this EDP, however, it requires the panel zones to remain elastic in the retrofitted scheme for LS1, therefore, it is assumed that the shear strain (or equivalent rotation) capacity limit for this EDP at LS1 is equivalent to γ_y (*i.e.*, no plastic deformation). Table 7 summarizes the shear strain capacity limits for the different codes, given in terms of equivalent plastic rotation. Figure 6 shows a comparison between the equivalent plastic rotation limit for the panel zones in function of ν_G.

Table 7. Equivalent plastic rotation capacity as consequence of shear strain in panel zones.

Code	Dimensionless axial load limits	Plastic shear strain capacity limit		
		LS1	**LS2**	**LS3**
EC8-3 [13]	None	0	Not specified	Not specified
ASCE 41-06 [15]	None	$1.0\ \theta_y$	$8.0\ \theta_y$	$11.0\ \theta_y$
ASCE 41-13 [18]	None	$1.0\ \theta_y$	$12.0\ \theta_y$	$12.0\ \theta_y$
ASCE 41-17 [19] [1]	$\lvert\nu_G\rvert < 0.4$	$1.0\ \theta_y$	$12.0\ \theta_y$	$12.0\ \theta_y$
	$\lvert\nu_G\rvert \geq 0.4$	$(5/3)(1-\lvert\nu_G\rvert)\ \theta_y$	$20(1-\lvert\nu_G\rvert)\ \theta_y$	$20(1-\lvert\nu_G\rvert)\ \theta_y$

[1] $\theta_y \equiv \gamma_y$

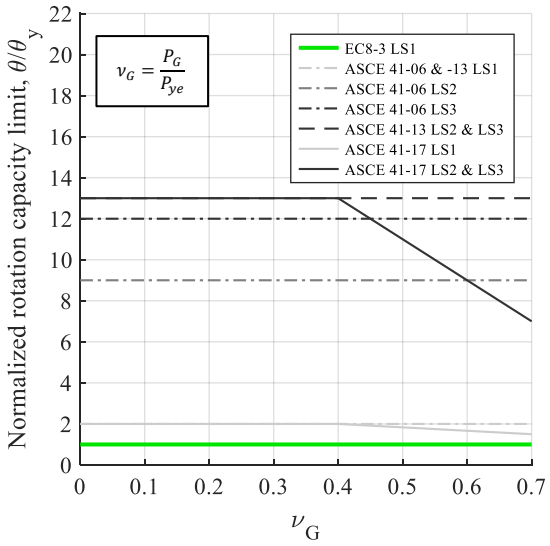

Figure 6. Normalized rotation capacity limits (θ/θ_y) for panel zones vs. dimensionless axial force ν_G.

3.3 Code-based global engineering demand parameters (EDPs)

One of the limitations in the use of local EDPs for the assessment of structures is the complexity of monitoring the components individually, especially when the assessment is done under multiple ground-motion sequences (*i.e.*, IDA). To overcome this issue, global EDPs, such as the IDR. are often used to synthetically describe the seismic response and indirectly monitor the demand imposed on the components. However, this approach could be suitable in new ductile structures designed by following modern seismic rules, that ensures well-established relationships between local failures and the global response, while may not be appropriate in existing buildings [33]. Some authors proposed mapping limits for global EDPs (such as for IDR) based on the demands imposed on local elements (*e.g.*, [44,45]) obtained through non-linear static analyses. Nonetheless, the relationship between global EDPs and the capacity of the local elements is not necessarily constant for all building typologies and geometries, which limits the direct use of global limits in a code-based framework. Moreover, this approach may be limited to low-rise buildings as it is affected by the assumption of the simplified analysis used, *i.e.*, distribution of forces according to the first mode of vibration in pushover analyses.

Despite the aforementioned limitations, the ASCE 41-06 [15] provided maximum inter-story drift ratio (MIDR) limits within the qualitative descriptions of the three limit states for steel MRFs, being 0.7%, 2.5% and 5%, for the LS1, LS2 and LS3, respectively.

Regardless of the capability of global EDPs to reflect component-level damage, they are key parameters in the estimation of non-structural damage, therefore, they become an important part of the performance-based assessment [4,5]. Both the MIDR and the maximum story acceleration (MSA) are often used as reference global EDPs, as large story deformations and accelerations have been related to damage of non-structural components (*e.g.*, partitions, ceilings, mechanical equipment, building contents).

Another important issue widely investigated in recent studies (*e.g.*, [44,46,47]) is related to the control of residual (*i.e.*, permanent) inter-story drift ratio (RIDR) which can compromise the building repairability [48]. The ASCE 41-06 [15] accounted for this issue by suggesting a negligible RIDR for LS1, a 1% RIDR for LS2 and a 5% RIDR for LS3.

Nonetheless, limit values for MIDR and RIDR are not provided in the newer versions of the code (*i.e.*, [18,19]). Despite not implemented in design or assessments codes, a RIDR limit of 0.5% is widely used for steel buildings in order to ensure the building repairability [48,49].

4. ASSESSMENT OF CASE STUDY BUILDINGS

For this paper, two of the SAC Steel Project [29] structures, particularly the pre-Northridge, 3- and 9-story Boston buildings, are used to carry out seismic assessments, in order to compare the code-established capacity values discussed in previous sections, within a probabilistic framework and by performing IDAs. It is worth emphasizing that the current study does not seek to assess the performance of specific structures, but instead treat these case study buildings as test-bed for the comparison of the codes, as these structures have been extensively investigated in literature (*e.g.*, [1]). These structures are representative of low- and mid-rise steel structures designed with low-ductility considerations. In addition, these pre-Northridge structures lack of capacity design considerations, similarly to those found in recently seismically reclassified European regions (*e.g.*, [2,6]). These buildings were chosen (1) for being representative of the ductility level of many steel MRFs in Europe and worldwide (*e.g.*, [2,6]); (2) for being extensively accepted and studied in literature [29]; and (3) for allowing the comparison of the ASCE 41-17 [19] with the rest of the codes, as the column's rotation capacity limits are calibrated on regressions made based on experiments performed on American W steel profiles.

4.1 Characteristics of the structures

The two case study buildings were designed as located in Boston (*i.e.*, low seismicity), built on stiff soil, designed for office occupancy, with regular plan distribution and with no considerable irregularities along the height. These buildings were intended to be representative of low- and mid-rise steel MRFs, (*i.e.*, 3 and 9 stories), and for the sake of brevity, they will be referred hereafter as 3B and 9B, respectively. Both structures were designed according to the 12th edition of the National Building Code (as noted by [29]), considering gravity, seismic and wind loads. Since the seismic demand for the site is very low, the seismic forces only controlled the design of 3B, while 9B design was controlled by wind loads [29]. In both cases, the lateral loads were resisted by perimeter steel MRFs, while the majority of the gravity loads were resisted by internal gravity frames, as it was common practice for this kind of structures in the early 90's in the USA. Similarly to Gupta and Krawinkler [29], this paper only considers the frames oriented on the N-S direction and neglects the torsional effects. Therefore, only the planar structure is analyzed with its corresponding tributary mass (*i.e.*, half of the building's mass). The plan views for buildings 3B and 9B are shown in Figure 7(a) and (b), respectively, while Figure 7(c) and (d) show the elevation of their studied frames. Building 9B is slightly modified from its original design, to remove the semi-pinned external span (from E to F), as its contribution to the lateral strength and stiffness is neglectable, therefore, it is simply considered to be part of the gravity system. The seismic mass for both buildings is reported in Table 8. For the assessment of the case study buildings, the beam-to-column connections are considered to be fully rigid, with no failure occurrence. Full knowledge of the structures (*i.e.*, $CF_{KLn} = 1$; $\kappa = 1$) is assumed in the case study buildings, as the goal is to compare the different EDPs in the different assessment codes.

4.2 Finite element (FE) models

Two-dimensional non-linear FE models of the frames were developed in OpenSees [50]. Columns are modelled based on the distributed plasticity approach to account for the interaction of axial and bending stresses. Beams are modelled based on the lumped plasticity approach (*i.e.*, non-linear rotational springs plus an elastic beam element). The plastic hinges on

549 the beams are calibrated based on the model proposed by Lignos and Krawinkler [51], modified under the approach
550 suggested by Zareian and Medina [52], in order to compensate the flexibility and the damping properties of the beams.
551 In addition, panel zones are modelled according to the 'Scissors model' [53], by using two parallel rotational springs.
552 Column bases are modelled as fixed for the 3B building, as previous studies [54] have suggested that the fixed base
553 assumption and detailed base plate models do not significantly differ on their contribution on the behavior of frames
554 designed to resist lateral loads. For the 9B building, column bases which are placed in the basement, are modelled as
555 pinned, as the interaction with the basement level lateral support, at ground level, provides a fixed effect, and the modeling
556 of the column base becomes almost irrelevant for the behavior of the structure. Column splices have been assumed as
557 fully rigid at this stage, and they are located in the middle of the column height, as in the original design of the case study
558 buildings [29]. The material properties are defined according to the design, *i.e.*, ASTM A572 Grade 50 (Group 1) steel in
559 all beams and columns (f_y = 344.74 MPa; E = 199.95 GPa). The nominal value of f_y is further increased by 10% to account
560 for the material overstrength, based on the recommendations made in ASCE 41-17 [19]. Damping is considered by using
561 mass- and stiffness proportional damping (*i.e.*, Rayleigh Damping), with a damping ratio ζ = 3%.
562
563 The effects of the gravity framing are included in the model by using a continuous leaning columns system, similar to
564 the ones proposed by MacRae *et al.* [55]. This column system is modelled in parallel to the structure and connected by
565 rigid links. The purposes of the leaning columns system are (1) to include the geometric second order effects (P-Δ) of the
566 gravity frame and (2) to provide lateral stiffness along the height of the structures. The latter issue is especially important
567 for low-code designed structures, as the stiffness of the gravity frame could represent a large portion of the overall lateral
568 stiffness. The columns in the system are individual fiber-based elements modelled in the same way as the columns of the
569 main system, but connected to the same nodes along the height, acting as a spine element for the structure. The effects of
570 the beam-to-column connections are neglected as they do not represent a significant contribution to the overall stiffness
571 of the structure [56]. One of the disadvantages of using the model outlined in MacRae *et al.* [55], is that the pinned column
572 base of the leaning columns system induces a concentration of base shear in the main frame of building 3B. To reduce
573 this effect, the strength and stiffness in the leaning columns' base plates is included by using simple rotational springs.
574 The design of the base plates was carried out following the AISC Steel Design Guide 1 [57], while the strength and
575 stiffness properties are defined based on the approach proposed by Kanvinde *et al.* [58].
576

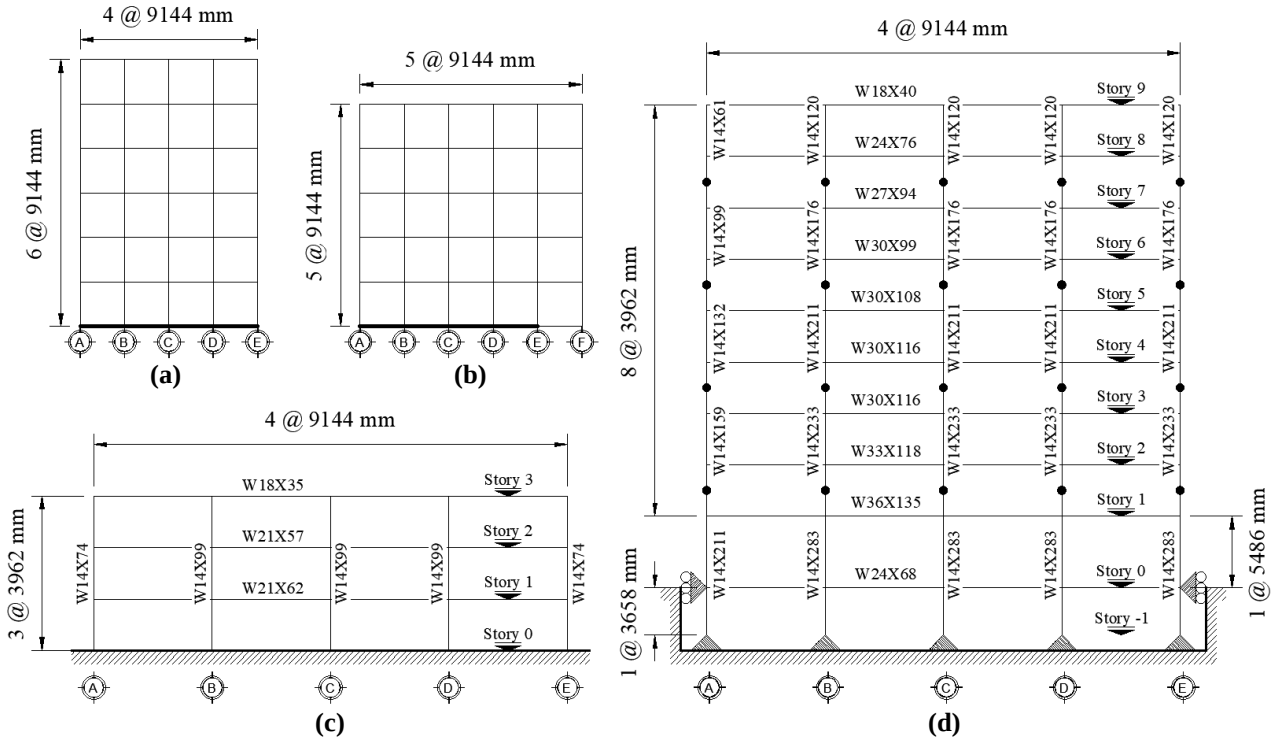

Figure 7. Plan view of (a) building 3B and (b) building 9B. Elevation view of N-S perimeter steel MRF for: (c) building 3B and (d) building 9B. (As reported in Gupta and Krawinkler [29]).

Table 8. Seismic masses per story for buildings 3B and 9B. Only the tributary masses are used for the models (*i.e.*, half of the reported mass).

Building 3B		Building 9B	
Story	**Mass [ton]**	**Story**	**Mass [ton]**
1	956.64	**1**	1009.19
2	956.64	**2 to 8**	991.73
3	1035.41	**9**	1069.29

4.3 Modal and non-linear static analyses

The first and second periods of vibration are respectively $T_{1\text{-}3B}$ = 1.88 sec and $T_{2\text{-}3B}$ = 0.52 sec for the building 3B and $T_{1\text{-}9B}$ = 3.21 sec and $T_{2\text{-}9B}$ = 1.18 sec for the building 9B. These periods are in agreement with previous studies (*i.e.*, [29]).

Non-linear static analyses, with lateral loads proportional to their first mode of vibration and story mass distribution, are performed to evaluate the capacity hierarchy of the elements, and the uniformity of story drifts along the height, as shown in Figure 8. Figure 8(a) and (b) show the results of the pushover analyses, in terms of IDR vs. story shear, respectively for buildings 3B and 9B. Markers are placed to identify simultaneous instants of the pushover analysis at each story. The IDRs of the building 3B is similar among its stories at different stages of the pushover analysis. The ductility of the structure is provided by the yielding of columns at the base of the structure, and the yielding of either the panel zones or the beam plastic hinges. Conversely, the building 9B shows a different distribution of the IDRs among its

stories, with drift concentrations in the middle levels (*i.e.*, levels 4, 5 and 6). For this building, the ductility is provided by the yielding in the panel zones and beams' plastic hinges through the building, and the large elastic and inelastic rotations of the columns in the first few stories.

Figure 8 also shows the yielding of the different structural components at different instants of the pushover analysis, represented by same color markers and correlated with Figure 8(c), (d) and (e) for 3B, and (f), (g) and (h) for 9B. The yellow color represents the instant on which the first element yielding occurs, which corresponds to the panel zones in the first story in 3B, and the panel zones in the fourth story in 9B. At this stage, the rest of the elements in the structure (*i.e.*, not yielded elements) control the IDR at all stories. Successively, the orange color represents the instant on which the first column yields (*i.e.*, the first fiber yields). In the case of 3B, all the column bases yield almost simultaneously, while in the case of 9B, the first column to yield is the most compressed column between the second and third stories, however. At this point, most of the beam-to-column joints have yielded in either the beam's plastic hinges or the panel zones. Finally, the red color represents the instant at which all beam-to-column joints have yielded in 3B, including joints in the roof, and the final yielding mechanism of the structure is developed. In the case of 9B, this stage is characterized by the yielding of most columns between the first and third stories, which enables the final yielding mechanism of the structure.

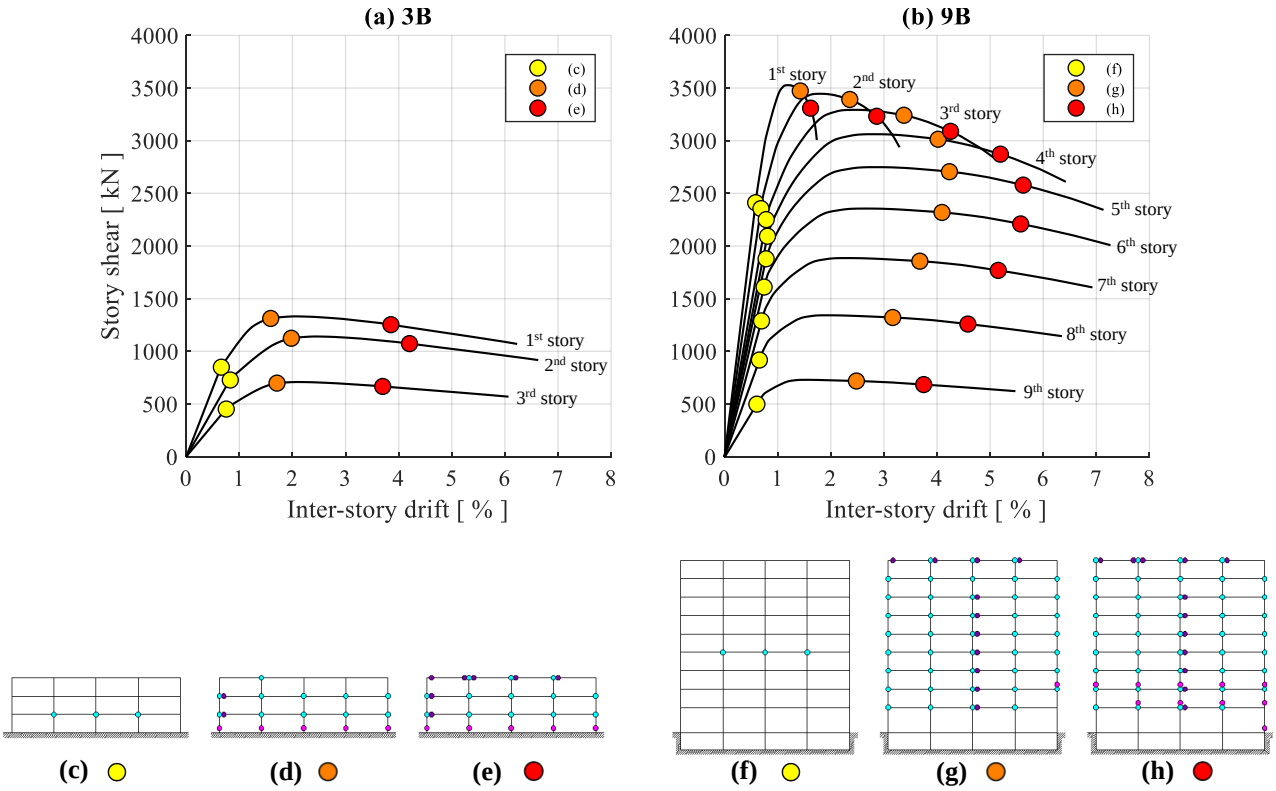

Figure 8. Pushover curves for: (a) building 3B; and (b) building 9B. (c), (d) and (e) show the progressive yielding of the structural elements for the building 3B, at the instants indicated in (a). (f), (g) and (h) show the progressive yielding of the structural elements for the building 9B, at the instants indicated in (b). Magenta circles represent yielding in columns; purple circles represent yielding in beams; cyan circles represent yielding in panel zones.

Although these curves are not intended to predict partial or total collapse of the structure, they provide a better understanding of the deformation mechanisms that these structures will likely follow. For 3B, the IDR is similar along the stories through the pushover analysis. However, for 9B, the IDR reflects only a partial picture of the overall deformation state in the structure. As it can be observed, middle stories (4th, 5th and 6th) show the highest IDR during the analysis due to the low capacity of the beam-to-column joints, which reduce the framing capacity of these levels. However, column yielding in 9B is concentrated in lower levels, which enables the middle levels to have higher IDR without being reflected in the chord rotation of the columns at this height, as the inclination angle is dragged from the bottom stories. Although the bottom columns (*i.e.*, between stories 0 and 1 in Figure 7) allow significant rotations, they do not necessarily develop large plastic deformation, since they are connected to relatively flexible panel zone springs at story 0, which provide a pinned-like support, as observed in Figure 8(h).

4.4 Ground motion input for the IDA

A set of 22 recorded far-field ground motions (GMs) developed in the ATC-63 project [59] is used for the non-linear time history analyses and to perform IDAs [59]. The GMs were recorded on stiff soil and do not exhibit pulse-type characteristics (*i.e.*, source-to-site distance higher than 10 km). This non-site-specific set of ground motions is selected in order to provide a test-bed for the comparison of the assessment codes applied on low-code structures, therefore, the study is not intended to describe the performance of a specific structure nor to assess for specific site demands. The average spectral acceleration (avgS_a) [60] for periods between $0.2T_{1\text{-}3B}$ and $1.5T_{1\text{-}9B}$ is used as IM. This choice was driven by the following considerations: (1) it is a structure-dependent IM; (2) it avoids the sensitivity caused by using scales based on high periods such as $T_{1\text{-}9B}$ (*i.e.*, to avoid that small variations in the scale factor result on unrealistically spectral acceleration values in higher modes [60]); and (3) it allows the direct comparison of the fragility curves between the two structures. The GMs were further scaled to different values of IM, from avgS_a equal to 0.02g to 1.0g, for a total of 1100 analyses for each case study structure. Figure 9 shows the 3% damping response spectra for the 22 GMs, scaled to match an avgS_a equal to 1.0g.

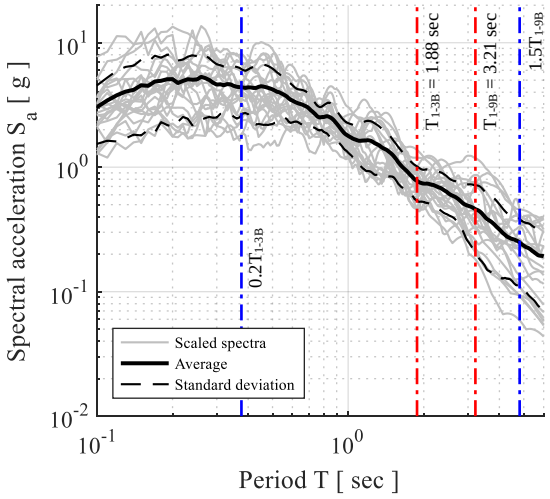

Figure 9. Response spectra for the 22 ground motions considering 3% damping.

4.5 Influence of the overturning axial loads in the yield rotation capacity of fiber-based modelled columns

As the capacity values are often established in terms of the yield capacity of the members, the calculation of θ_y plays a crucial role in the assessment of structural elements, particularly those in which the yield capacity is function of the demand, such as the columns. In order to allow the comparison of these code-based parameters, a probabilistic approach is required to account for the record-to-record variability in the yield rotation capacity of the columns. Therefore, a set of fragility curves, fitted by analytical lognormal curves obtained through least-square minimization, is derived to represent the probability of failure (*i.e.*, demand rotation > yielding rotation) conditioned to the IM, $P(\theta \geq \theta_y \mid IM)$, as observed in Figure 10. The assumption of lognormality simplifies the analysis of the results and allows the description of the fragility functions in two synthetic parameters: the median fragility capacity IM_{50} (*i.e.*, the IM corresponding to 50% probability of exceedance), and the standard deviation β [33], which are reported in Table 9. In addition to the fragility curves parameters, Table 9 shows a comparison between IM_{50} with respect to the fiber-based model.

Fragility curves to represent the $P(\theta \geq \theta_y \mid IM)$ for each individual column ends are derived to identify the most fragile fiber-based column elements. The value of θ_y is established as the chord rotation when the first column fiber yields. As it can be observed in Figure 10(a), the columns in the base of 3B are the most fragile. In a similar way, Figure 10(b) shows that the columns above the base of 9B (*i.e.*, columns between stories 0 and 1) are the most fragile, however, unlike 3B, they exhibit a similar probability of yielding as other columns, due to their lack of fixed supports at the base.

Fragility curves to represent all the $P(\theta \geq \theta_y \mid IM)$ in all the columns are derived (*i.e.*, the failure in one component is considered as the column system failure). First, similarly to the individual fragility curves, the value of θ_y is established based on the fiber model. Then, different values of θ_y corresponding to Eqs. 1, 2 and 3, are used to represent the fragility according to the EC8-3 [13], the ASCE 41-06/13 [15,18] and the ASCE 41-17 [19], respectively. Moreover, the definition of θ_y proposed by Lignos *et al.* [42] is used as an experimental-based reference, as it is defined on regression models based on results from experimental campaigns and numerical simulations on W steel sections. In addition, a fragility curve to represent the fiber-based yielding of columns in internal axes (*i.e.*, first column to yield within axes B, C and D) is derived for 9B, to represent the fragility of those columns that are not significantly affected by overturning effects (*i.e.*, mostly gravity axial loads considered).

As it can be observed in Figure 10(a), for building 3B, the fragility curve derived from the fiber-based θ_y, is similar to the fragility curve derived by using the parameters proposed by Lignos *et al.* [42] (only 11% difference in IM_{50} with respect to the fiber-based model). However, the difference becomes larger in the case of building 9B in Figure 10(b), for which the fiber-based fragility curve derived for all columns differs significantly from the fragility curve derived by using the parameters proposed by Lignos *et al.* [42] (21% difference in IM_{50} with respect to the fiber-based model). Nonetheless, when only internal columns are considered, the correspondence is significantly increased (3% difference in IM_{50} in the curves derived based on Lignos *et al.* [42] limits, with respect to the fiber-based internal columns). This discrepancy may be related to the use of gravity axial loads only in the relationship proposed by Lignos *et al.* [42] to establish values for θ_y, which is a similar case to the internal columns as they have a lower affectation from the overturning effects). With respect to the θ_y defined as in the codes, none of them are able to match the fragility curves derived based on the fiber-based elements or the parameters proposed by Lignos *et al.* [42], with the ASCE 41-06 and 13 [15,18] exhibiting more

conservative results (*i.e.*, higher fragility), while the EC8-3 [13] and ASCE 41-17 [19] show less conservative values (*i.e.*, lower fragility).

Table 9. Fragility curves parameters for $P(\theta \geq \theta_y \mid IM)$.

θ_y calculation approach	Building 3B		Building 9B	
	IM_{50} [g]	β [-]	IM_{50} [g]	β [-]
EC8-3 [13]	0.220 (+80%)	0.276	0.805 (+85%)	0.187
ASCE 41-06/13 [15,18]	0.085 (-33%)	0.220	0.269 (-38%)	0.184
ASCE 41-17 [19]	0.313 (+157%)	0.256	0.912 (+110%)	0.271
Fiber-based model (all columns)	0.122	0.146	0.435	0.274
Fiber-based model (internal columns)	0.122 (0%)	0.146	0.514 (+18%)	0.210
Lignos *et al.* [42]	0.136 (+11%)	0.229	0.528 (+21%)	0.260

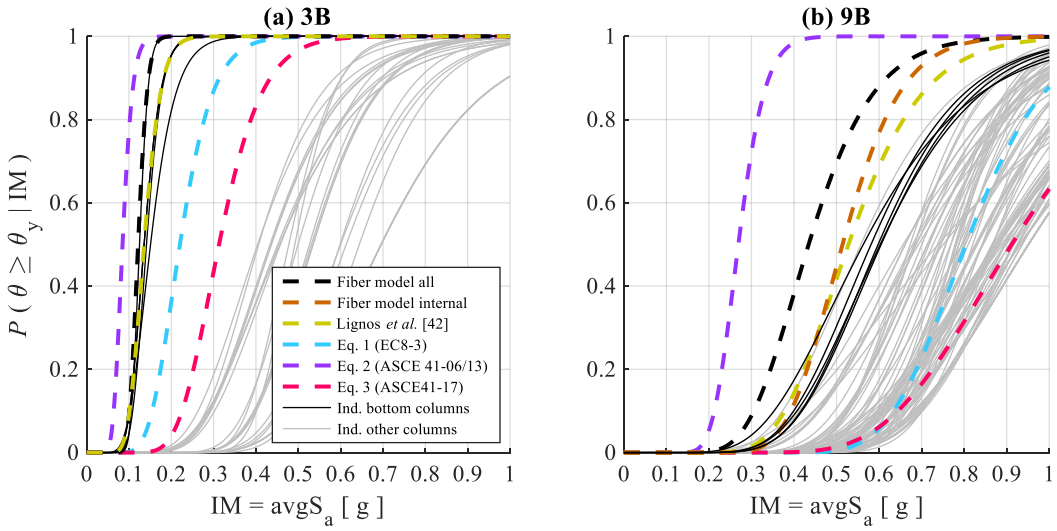

Figure 10. Comparison of fragility curves based on the $P(\theta \geq \theta_y \mid IM)$ for 3B (a) and 9B (b). The solid lines represent the fragility curves for individual fiber-based column elements, while the broken lines represent the fragility curves for all the columns in the building together, according to various definitions of θ_y.

4.6 Fragility based on the code-established limit states

Fragility curves are derived for each local EDP, code and limit state, for comparisons between the capacity values established by the codes. While accounting for the uncertainty related to the seismic demand (*i.e.*, record-to-record variability), the variation of demand-dependent capacity values is implicitly considered (*i.e.*, θ_y in the columns). The seismic demand is monitored for each EDP and each component and compared to the seismic capacity determined by the values described in Section 3. A given limit state is considered overpassed when one or more elements surpass the deformation capacity limit attained to it, in accordance with the failure criteria established in the assessment codes [13,15,18,19]. As the W14×61 column in 9B is considered 'Class 3' in the EC3-1-1 [43], this column is not considered in the assessment as it should be treated as force-controlled element, which would limit the comparison between codes.

In addition, the force-controlled actions, such as shear in beams and columns, are checked a-posteriori and none of them rules the capacity of the structure at any point.

A comparison of the fragility curves for the different components and for the system (*i.e.*, the first element, of any kind, to overpass the limit state) for 3B is presented in Figure 11(a) to (d), while the fragility curves corresponding to 9B are shown in Figure 11(e) to (h). In addition, a reference set of fragility curves based on the MIDR limits established by ASCE 41-06 [15] is included in all the figures to enable the comparison of the local EDPs to a constant global EDP, and to facilitate the comparison between different EDPs. These fragility curves are representative of MIDRs limits of 0.7%, 2.5% and 5.0%, for the LS1, LS2 and LS3, respectively. The median fragility capacity IM_{50} for all EDPs, limit states and assessment codes, for both buildings is presented in Table 10, as well as a comparison with respect to EC8-3 [13]. Some of the fragility curves seem to be similar in different codes and limit states at higher levels of IM (*e.g.*, beams and columns rotation in 9B), however, this is only because the numerical model cannot longer converge and all elements are considered to overpass all limit states (*i.e.*, collapse is presumed).

Table 10. Median fragility capacity IM_{50} for all EDPs, limit states and assessment codes, for buildings 3B and 9B.

		Building 3B[1,2]				Building 9B[1,2]			
	Limit state	**EC8-3** [13]	**ASCE 41-06** [15]	**ASCE 41-13** [18]	**ASCE 41-17** [19]	**EC8-3** [13]	**ASCE 41-06** [15]	**ASCE 41-13** [18]	**ASCE 41-17** [19]
Beams Rotation	**LS1**	0.342	**0.337** (-1%)	**0.337** (-1%)	0.490 (+43%)	0.407	**0.400** (-2%)	**0.400** (-2%)	0.640 (+57%)
	LS2	0.632	**0.625** (-1%)	0.680 (+8%)	0.673 (+6%)	0.936	**0.931** (-1%)	0.947 (+1%)	0.947 (+1%)
	LS3	**0.660**	**0.660** (0%)	0.696 (+5%)	0.696 (+5%)	**0.947**	**0.947** (0%)	0.951 (0%)	0.951 (0%)
Columns Rotation	**LS1**	0.311	**0.105** (-66%)	**0.105** (-66%)	0.392 (+26%)	0.888	**0.557** (-37%)	**0.557** (-37%)	0.951 (+7%)
	LS2	0.546	**0.316** (-42%)	0.403 (-26%)	0.580 (+6%)	0.951	0.951 (0%)	0.951 (0%)	0.951 (0%)
	LS3	0.591	**0.403** (-32%)	0.448 (-24%)	0.601 (+2%)	0.951	0.951 (0%)	0.951 (0%)	0.951 (0%)
Panel Zones Strain	**LS1**	**0.086**	0.113 (+31%)	0.113 (+31%)	0.118 (+37%)	**0.093**	0.109 (+17%)	0.109 (+17%)	0.136 (+46%)
	LS2	-	**0.346**	0.439	0.501	-	**0.340**	0.489	0.574
	LS3	-	**0.427**	0.439	0.501	-	**0.445**	0.489	0.574
System	**LS1**	**0.086**	0.106 (+23%)	0.106 (+23%)	0.118 (+37%)	**0.093**	0.109 (+17%)	0.109 (+17%)	0.136 (+46%)
	LS2	0.546	**0.312** (-43%)	0.398 (-27%)	0.501 (-8%)	0.936	**0.340** (-64%)	0.489 (-48%)	0.574 (-39%)
	LS3	0.591	**0.398** (-33%)	0.433 (-27%)	0.501 (-15%)	0.947	**0.445** (-53%)	0.489 (-48%)	0.574 (-39%)

[1] Bold values represent the most conservative code for that EDP and limit state, underlined values represent the least conservative code.

[2] The quantities in parenthesis represent the change with respect to the EC8-3 [13].

Based on Figure 11 and Table 10 the following observations can be made:

- The rotation in beams was not critical in any case, as the flexibility of panel zones avoid the early development of plastic hinges in beams, as displayed in Figure 11(a) and (e). This is consistent with frames designed with no capacity design considerations.
- The plots of Figure 11(b) demonstrate that the columns in 3B are among the most fragile elements in the system, particularly for the ASCE 41-06 and -13 [15,18], due to the consideration of the axial loads in the derivation of θ_y. On the other hand, as in Figure 11(f), the columns of 9B did not exhibit high levels of demand, except in LS1 for the ASCE 41-06 and -13 [15,18]. This is due to the larger yield rotation capacity of the columns, as a consequence of the basement level (which acts as a partially-fixed column base).
- As can be observed in Figure 11(d) and (h), the system fragility is controlled by the panel zones in most cases for both buildings, except when no capacity limits are provided for panel zones (*i.e.*, LS2 and LS3 in EC8-3 [13]) and in a few cases in which the columns rules the system capacity at some levels of IM (*i.e.*, LS2 and LS3 in ASCE 41-06/13 [15,18] for 3B), mainly due to the different definition of θ_y.
- If the EC8-3 [13] restriction of developing plastic deformation in panel zones at LS1 is considered, the most conservative system assessment for LS1 is indeed found under the EC8-3 [13] regulations, as observed in Figure 11(d) and (h). For this limit state, the median fragility capacity IM_{50} of the ASCE 41-06, -13 and -17 [15,18,19] result on differences of 31%, 31% and 37% for 3B, and 17%, 17% and 46% for 9B, with respect to the EC8-3 [13].
- When the assessment for LS2 and LS3 is made under the regulations of the EC8-3 [13] the results are the least conservative in comparison with all the versions of ASCE 41 [15,18,19], due to the lack of code-established capacity limits for panel zones. With respect to the EC8-3 [13], the median fragility capacity IM_{50} for the ASCE 41-06, -13 and -17 [15,18,19] result on differences of 43%, 27% and 8% for LS2 in 3B; 33%, 27% and 15% for LS3 in 3B; 64%, 48% and 39% for LS2 in 9B; and 53%, 48% and 39% for LS3 in 9B.
- When the fragility of 3B in Figure 11(d) is compared to the fragility of 9B in Figure 11(h), 3B results on a more fragile structure, except for LS1, in which both structures exhibit similar levels of fragility. However, this is heavily influenced by the differences in spectral accelerations due to the location of the fundamental period in the spectra.
- Among the American codes, the newer versions of the prescription have shifted towards less conservative assessment outcomes in all cases.

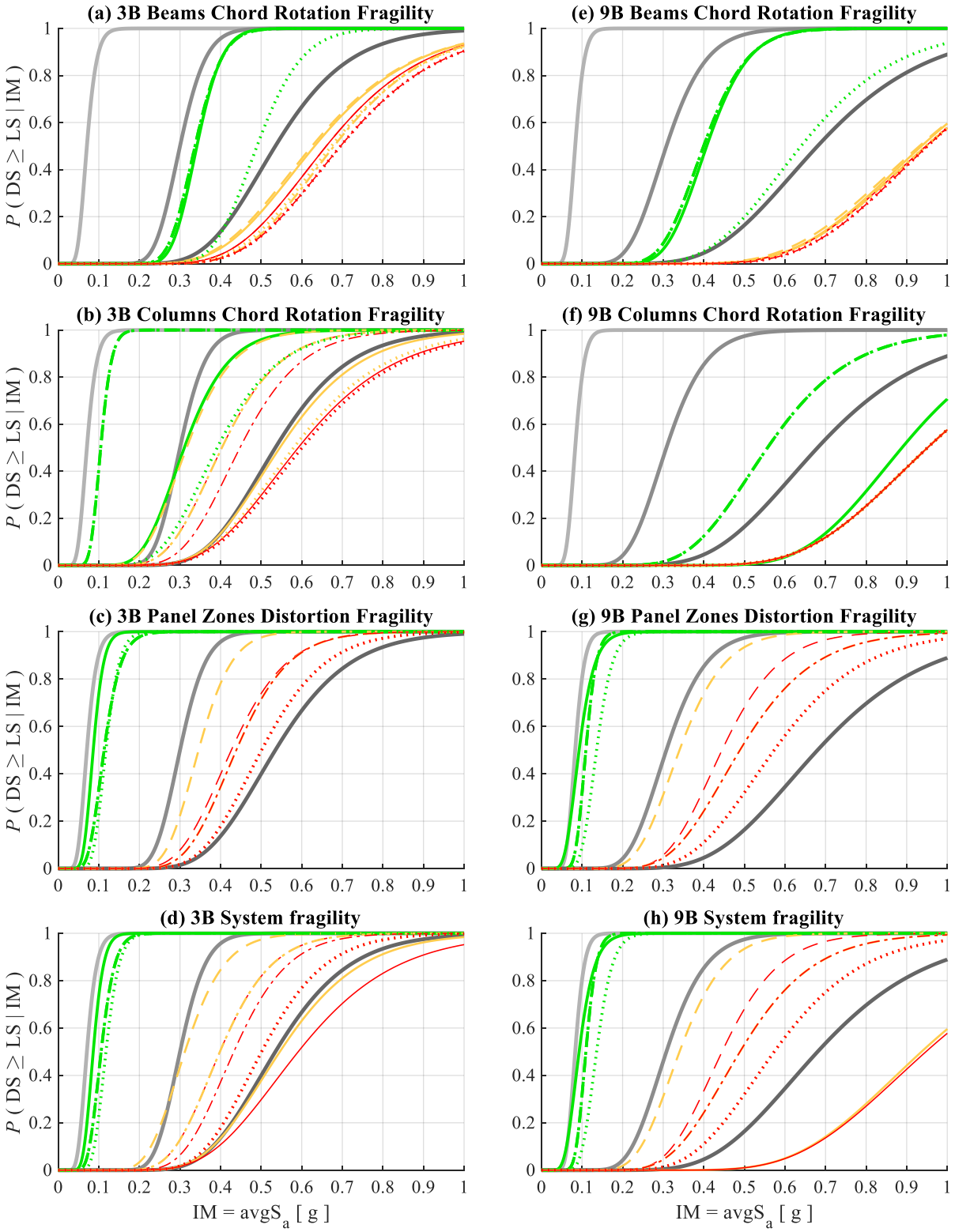

Figure 11. Comparison of fragility curves for different EDPs for buildings 3B and 9B, based on the procedures of the different considered codes.

4.7 Global EDPs

In parallel to the assessment of the local components, fragility curves for the MIDR, RIDR and MSA are provided and shown in Figure 12. The fragility curves for MIDRs (shown also in Figure 11) are derived for 0.7%, 2.5% and 5%, which correspond with the limits established by the ASCE 41-06 [15] for the LS1, LS2 and LS3. The fragility curve for the RIDR is derived for 0.5%, based on the considerations highlighted by McCormick [48]. Finally, fragility curves for MSA are derived based on the four thresholds considered by the HAZUS MR4 Manual [61] for low-code structures: 0.20g (Slight), 0.40g (Moderate), 0.8g (Extensive) and 1.6g (Complete). As observed in Figure 12, fragility curves for the 0.7% MIDR and 0.20g MSA, tend to exhibit similar median and dispersion values. This is also observed in the fragility curves corresponding to the highest global damage levels (*i.e.*, 5% MIDR and 1.6g MSA). Finally, the fragility curves for the intermediate global damage levels, including the 2.5% MIDR, 0.5% RIDR and 0.8g MSA, exhibit median values which roughly correspond to an IM = 0.3g in both cases, nonetheless, the 0.5% RIDR and 0.8g MSA fragility curves display a larger dispersion.

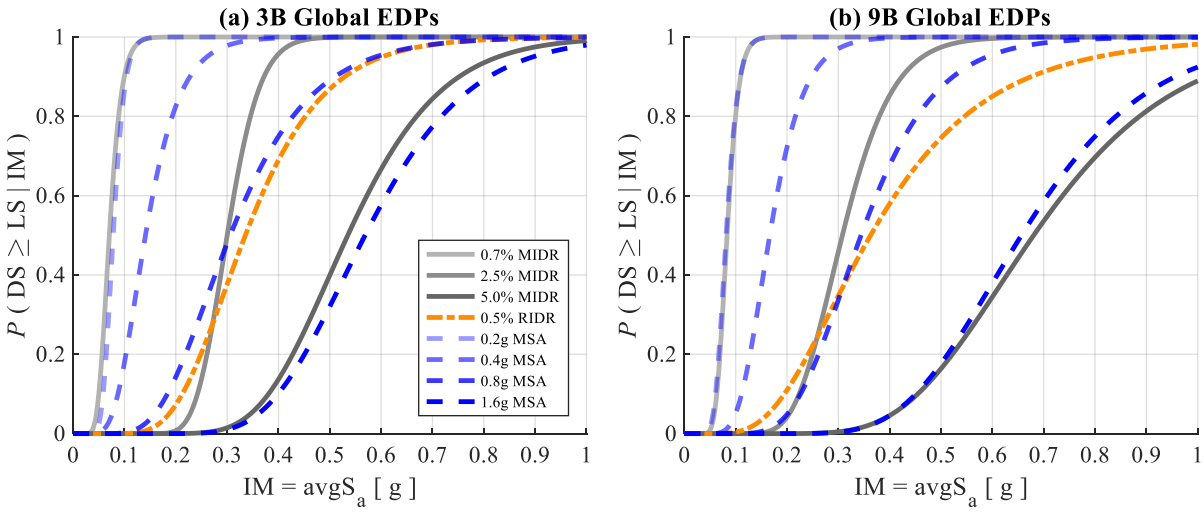

Figure 12. Comparison of fragility curves for different global EDPs for buildings 3B and 9B.

5. CONCLUSIONS

This paper presents a detailed comparison between the Eurocode 8 – Part 3 (EC8-3) [13] and the American ASCE 41 [15,18,19] assessment codes, focusing on the use of the most relevant engineering demand parameters in the assessment of existing steel moment resisting frames. Several similarities and differences were identified by comparing the EC8-3 [13] to its American peers, providing insights and directions for development of the EC8-3.

One of the main identified drawbacks of the EC8-3 [13] is related to the lack of explicit assessment tools for strain in panel zones, other than the conservative limitation of keeping panel zones within the elastic range for the Damage Limitation limit state (LS1). This limitation is equivalent to 50% of the deformation allowance established in the ASCE 41 [15,18,19] for the equivalent limit state (Immediate Occupancy). Therefore, from one side, the lack of parameters for LS2 and LS3 does not allow the control of this failure mode which would result in more conservative assessment in certain cases (*e.g.*, LS1), while being less conservative in others (*e.g.*, LS2 and LS3 in low-code buildings with no capacity design considerations), in comparison with the ASCE 41 [15,18,19].

In order to allow the comparison for capacity limits in beams and columns, a significant effort was made for the normalization of the capacity limits considering the slenderness parameters and code definitions of θ_y. The capacity values established by the EC8-3 [13] tend to be more conservative than those established by the ASCE 41 [15,18,19]. Nonetheless, this is not always the case, as the capacity values are established as a function of the slenderness parameters and, in some cases, the dimensionless axial force ν. For example, in a comparison between the EC8-3 [13] and ASCE 41-17 [19] capacity values for a W14×283 column section with $\nu = \nu_G = 0.1$, the capacity values in the ASCE 41-17 [19] are increased by 133%, 95% and 99% for LS1, LS2 and LS3, respectively, with respect to those of the EC8-3 [13]. Nevertheless, when considering a W14×74 section instead, the capacity value is increased by only 12% for LS1, while a reduction of 16% and 17% is calculated for LS2 and LS3. It is worth highlighting that both sections are classified as 'Class 1' in the Eurocode 3 - Part 1-1 [43].

The discrete definition of the capacity values based on slenderness limits for the classification of beam and column sections in EC8-3 [13] may be appropriate to influence design decisions for new structures, as the designer can simply consider or discard a section depending on its class. However, this discretized approach may not be appropriate in the assessment of an existing structure, while a more continuous classification would allow to reduce the conservativeness in the classification. On the other hand, the ASCE 41 [15,18,19] establishes continuous capacity limits that are directly function of the slenderness parameters, which avoids the inconveniences of the strict discrete class-dependent approach used by the EC8-3 [13]. In a similar way, those columns with dimensionless axial load $\nu > 0.3$ are treated as force-controlled elements in the European regulation, which may significantly reduce the system capacity in some cases. The ASCE 41-06 and -13 [15,18], on the other hand, allow columns with values of $\nu \leq 0.5$ to be considered as deformation-controlled, while the ASCE 41-17 [19] pushes the limit further to $\nu_G \leq 0.6$.

The current version of the EC8-3 [13] lacks of explicit modeling parameters for the different components, including monotonic and cyclic deformations. Following the trend established by the ASCE 41-17 [19], the new version of the EC8-3 could incorporate modeling parameters and capacity limits based on experiments performed on European steel sections and materials (*e.g.*, [23–26]), which also considered the effect of axial loads, section and member slenderness.

To gain additional insights on the influence of the different definition of the capacity limits, two case study buildings have been selected and analyzed by performing Incremental Dynamic Analyses (IDA) and developing fragility curves. The direct comparison of the assessment codes shows that the EC8-3 [13] is conservative for LS1 and unconservative for LS2 and LS3, when compared to the American codes [15,18,19]. This is mainly due to the lack of panel zone's capacity limits, but also to the lack of consideration of axial load demands in the columns. This difference is more significant in taller structures, as the relative axial loads are usually increased. The comparison of the system fragility curves allows the quantification of the differences on the two case studies analyzed. The EC8-3 [13] provides conservative results for LS1 when compared to the American codes, *i.e.*, the IM corresponding to 50% probability of exceedance, IM_{50} for LS1 are 23%, 23% and 37% higher than the EC8-3 [13] respectively for ASCE 41-06 [15], -13 [18] and -17 [19] in the building 3B; and 17%, 17% and 46% higher in the building 9B. These differences are mainly due to the restriction of developing plastic deformation in the panel zones. On the other hand, the assessment for LS2 and LS3 performed with the EC8-3 [13] resulted in unconservative estimates of the fragilities when compared with the American codes, *i.e.*, IM_{50} values are 43%, 27% and 8% smaller for LS2, and 33%, 27% and 15% for LS3, for building 3B; while higher differences are

observed in building 9B, *i.e.*, IM_{50} values are 64%, 48% and 39% smaller for LS2 and 53%, 48% and 39% smaller for LS3. These differences are as well, related to the lack of capacity limits for panel zones and the lack of considerations of the axial load demands in the columns in the EC8-3 [13].

ACKNOWLEDGEMENTS

This research was partially funded by CONACYT-FiiDEM (Grant No. 2018-000013-01EXTF-00148). Any opinions, findings, and conclusions or recommendations expressed in this paper are those of the authors and do not necessarily reflect the views of the funding agencies.

REFERENCES

[1] Federal Emergency Management Agency, State of the Art Report on Systems Performance of Steel Moment Frames Subject to Earthquake Ground Shaking, FEMA 355C. (2000).

[2] L. Di Sarno, F. Paolacci, A.G. Sextos, Seismic performance assessment of existing steel buildings: A case study, Key Eng. Mater. 763 (2018) 1067–1076. https://doi.org/10.4028/www.scientific.net/KEM.763.1067.

[3] E. Tapia-Hernández, J.S. García-Carrera, Damage assessment and seismic behavior of steel buildings during the Mexico earthquake of 19 September, Earthq. Spectra. 36 (2020) 250–270. https://doi.org/10.1177/8755293019878186.

[4] European Committe for Standarization, Eurocode 8: Design of structures for earthquake resistance - Part 1: General rules, seismic actions and rules for buildings, EN 1998-1. (2004).

[5] American Society of Civil Engineers, Minimum Design Loads and Associated Criteria for Buildings and Other Structures, ASCE/SEI 7-16. (2017). https://doi.org/10.1061/9780784414248.

[6] L. Di Sarno, J.R. Wu, Seismic assessment of existing steel frames with masonry infills, J. Constr. Steel Res. 169 (2020) 106040. https://doi.org/10.1016/j.jcsr.2020.106040.

[7] M. Araújo, J.M. Castro, A Critical Review of European and American Provisions for the Seismic Assessment of Existing Steel Moment-Resisting Frame Buildings, J. Earthq. Eng. 22 (2018) 1336–1364. https://doi.org/10.1080/13632469.2016.1277568.

[8] Federal Emergency Management Agency, State of the Art Report on Past Performance of Steel Moment-Frame Buildings in Earthquakes, FEMA 355E. (2000).

[9] Applied Technology Council, Evaluating the Seismic Resistance of Existing Buildings, ATC-14. (1987).

[10] R. Pekelnicky, C. Poland, ASCE 41-13: Seismic Evaluation and Retrofit Rehabilitation of Existing Buildings, in: SEAOC 2012 Conv. Proc., 2012: pp. 1–12.

[11] M.N. Fardis, Current Developments and Future Prospects of the European Code for Seismic Design and Rehabilitation of Buildings: Eurocode 8, 13th World Conf. Earthq. Eng. 2 (2004) 15.

[12] European Committe for Standarization, Eurocode 8: Design Provisions for Earthquake Resistance of Structures. General Rules - Strengthening and Repair of Buildings, ENV 1998-1-4. (1996).

[13] European Committe for Standarization, Eurocode 8: Design of Structures for Earthquake Resistance - Part 3: Assessment and Retrofitting of Buildings, EN 1998-3. (2005).

[14] Federal Emergency Management Agency, Prestandard and Commentary for the Seismic Rehabilitation of Buildings, FEMA 356. (2000).

[15] American Society of Civil Engineers, Seismic Rehabilitation of Existing Buildings, ASCE/SEI 41-06. (2007).

https://doi.org/10.1061/9780784408841.
[16] American Society of Civil Engineers, Seismic Evaluation of Existing Buildings, ASCE/SEI 31-03. (2003). https://doi.org/10.1061/9780784406700.
[17] American Society of Civil Engineers, Minimum Design Loads for Buildings and Other Structures, ASCE/SEI 7-10. (2010). https://doi.org/10.1061/9780784412916.
[18] American Society of Civil Engineers, Seismic Evaluation and Retrofit of Existing Buildings, ASCE/SEI 41-13. (2014). https://doi.org/10.1061/9780784412855.
[19] American Society of Civil Engineers, Seismic Evaluation and Retrofit of Existing Buildings, ASCE/SEI 41-17. (2017). https://doi.org/10.1061/9780784414859.
[20] R. Pekelnicky, G. Hagen, D. Martin, A Summary of Significant Updates in ASCE 41-17, SEAOC 2017 Conv. Proc. (2017).
[21] D. Bech, J. Houston, B. Tremayne, ASCE 41-17 Steel Column Modeling and Acceptance Criteria, in: Struct. Congr. 2017, 2017.
[22] M. Araújo, J.M. Castro, On the quantification of local deformation demands and adequacy of linear analysis procedures for the seismic assessment of existing steel buildings to EC8-3, Bull. Earthq. Eng. 14 (2016) 1613–1642. https://doi.org/10.1007/s10518-016-9897-4.
[23] J. Cravero, A. Elkady, D.G. Lignos, Experimental Evaluation and Numerical Modeling of Wide-Flange Steel Columns Subjected to Constant and Variable Axial Load Coupled with Lateral Drift Demands, J. Struct. Eng. 146 (2020) 1–19. https://doi.org/10.1061/(ASCE)ST.1943-541X.0002499.
[24] M. D'Aniello, R. Landolfo, V. Piluso, G. Rizzano, Ultimate behavior of steel beams under non-uniform bending, J. Constr. Steel Res. 78 (2012) 144–158. https://doi.org/10.1016/j.jcsr.2012.07.003.
[25] M. Araújo, L. Macedo, J.M. Castro, Evaluation of the rotation capacity limits of steel members defined in EC8-3, J. Constr. Steel Res. 135 (2017) 11–29. https://doi.org/10.1016/j.jcsr.2017.04.004.
[26] D.G. Lignos, A.R. Hartloper, Steel column stability and implications in the seismic assessment of steel structures according to Eurocode 8 Part 3, Stahlbau. 89 (2020) 16–27. https://doi.org/10.1002/stab.201900108.
[27] R. Montuori, E. Nastri, V. Piluso, P. Todisco, A simplified performance based approach for the evaluation of seismic performances of steel frames, Eng. Struct. 224 (2020) 111222. https://doi.org/10.1016/j.engstruct.2020.111222.
[28] H. Krawinkler, S. Mohasseb, Effects of panel zone deformations on seismic response, J. Constr. Steel Res. 8 (1987) 233–250. https://doi.org/10.1016/0143-974X(87)90060-5.
[29] A. Gupta, H. Krawinkler, Behavior of Ductile SMRFs at Various Seismic Hazard Levels, J. Struct. Eng. 126 (2000) 98–107.
[30] C. Molina Hutt, T. Rossetto, G.G. Deierlein, Comparative risk-based seismic assessment of 1970s vs modern tall steel moment frames, J. Constr. Steel Res. 159 (2019) 598–610. https://doi.org/10.1016/j.jcsr.2019.05.012.
[31] A.K. Kazantzi, T.D. Righiniotis, M.K. Chryssanthopoulos, Fragility and hazard analysis of a welded steel moment resisting frame, J. Earthq. Eng. 12 (2008) 596–615. https://doi.org/10.1080/13632460701512993.
[32] M. Kia, M. Banazadeh, Closed-form fragility analysis of the steel moment resisting frames, Steel Compos. Struct. 21 (2016) 93–107. https://doi.org/10.12989/scs.2016.21.1.093.
[33] F. Freddi, E. Tubaldi, L. Ragni, A. Dall'Asta, Probabilistic performance assessment of low-ductility reinforced concrete frames retrofitted with dissipative braces, Earthq. Eng. Struct. Dyn. 42 (2013) 993–1011.

907 https://doi.org/10.1002/eqe.2255.
908 [34] D. Vamvatsikos, C. Allin Cornell, Incremental dynamic analysis, Earthq. Eng. Struct. Dyn. 31 (2002) 491–514.
909 https://doi.org/10.1002/eqe.141.
910 [35] F. Freddi, J.E. Padgett, A. Dall'Asta, Probabilistic seismic demand modeling of local level response parameters
911 of an RC frame, Bull. Earthq. Eng. 15 (2017). https://doi.org/10.1007/s10518-016-9948-x.
912 [36] B. Song, C. Galasso, A. Kanvinde, Advancing fracture fragility assessment of pre-Northridge welded column
913 splices, Earthq. Eng. Struct. Dyn. 49 (2020) 132–154. https://doi.org/10.1002/eqe.3228.
914 [37] R.A. Medina, H. Krawinkler, B. Alavi, Seismic demand for nondeteriorating frame structures and their
915 dependence on ground motion, 2003. https://doi.org/10.1016/S0141-0296(02)00174-8.
916 [38] O.S. Kwon, A. Elnashai, The effect of material and ground motion uncertainty on the seismic vulnerability curves
917 of RC structure, Eng. Struct. 28 (2006) 289–303. https://doi.org/10.1016/j.engstruct.2005.07.010.
918 [39] E. Tubaldi, M. Barbato, A. Dall'Asta, Influence of model parameter uncertainty on seismic transverse response
919 and vulnerability of steel-concrete composite bridges with dual load path, J. Struct. Eng. 138 (2012) 363–374.
920 https://doi.org/10.1061/(ASCE)ST.1943-541X.0000456.
921 [40] E. Tubaldi, F. Freddi, M. Barbato, Probabilistic seismic demand model for pounding risk assessment, Earthq.
922 Eng. Struct. Dyn. (2016). https://doi.org/10.1002/eqe.2725.
923 [41] V. Piluso, A. Pisapia, P. Castaldo, E. Nastri, Probabilistic Theory of Plastic Mechanism Control for Steel Moment
924 Resisting Frames, Struct. Saf. 76 (2019) 95–107. https://doi.org/10.1016/j.strusafe.2018.08.003.
925 [42] D.G. Lignos, A.R. Hartloper, A. Elkady, G.G. Deierlein, R. Hamburger, Proposed Updates to the ASCE 41
926 Nonlinear Modeling Parameters for Wide-Flange Steel Columns in Support of Performance-Based Seismic
927 Engineering, J. Struct. Eng. 145 (2019) 1–13. https://doi.org/10.1061/(ASCE)ST.1943-541X.0002353.
928 [43] European Committe for Standarization, Eurocode 3: Design of Steel Structures - Part 1-1: General Rules and
929 Rules for Buildings, EN 1993-1-1. (2005).
930 [44] E. Elettore, F. Freddi, M. Latour, G. Rizzano, Design and analysis of a seismic resilient steel moment resisting
931 frame equipped with damage-free self-centering column bases, J. Constr. Steel Res. (2021).
932 https://doi.org/10.1016/j.jcsr.2021.106543.
933 [45] K. Aljawhari, R. Gentile, F. Freddi, C. Galasso, Effects of ground-motion sequences on fragility and vulnerability
934 of case-study reinforced concrete frames, Springer Netherlands, 2020. https://doi.org/10.1007/s10518-020-
935 01006-8.
936 [46] F. Freddi, C.A. Dimopoulos, T.L. Karavasilis, Rocking damage-free steel column base with friction devices:
937 design procedure and numerical evaluation, Earthq. Eng. Struct. Dyn. 46 (2017) 2281–2300.
938 https://doi.org/10.1002/eqe.2904.
939 [47] F. Freddi, C.A. Dimopoulos, T.L. Karavasilis, Experimental Evaluation of a Rocking Damage-Free Steel Column
940 Base with Friction Devices, J. Struct. Eng. 146 (2020) 04020217. https://doi.org/10.1061/(asce)st.1943-
941 541x.0002779.
942 [48] J. McCormick, H. Aburano, M. Ikenaga, M. Nakashima, Permissible Residual Deformation Levels for Building
943 Structures Considering both Safety and Human Elements, 14th World Conf. Earthq. Eng. (2008) 8.
944 [49] Y. Iwata, H. Sugimoto, H. Kuwamura, Reparability limit of steel structural builidings : Study on performance
945 based design of steel structural buildings, Part 2, J. Struct. Constr. Eng. 70 (2005) 165–172.
946 https://doi.org/10.3130/aijs.70.165_1.

947 [50] F. McKenna, G.L. Fenves, M.H. Scott, Open system for earthquake engineering simulation (OpenSees), (2000).
948 [51] D.G. Lignos, H. Krawinkler, Deterioration modeling of steel components in support of collapse prediction of steel
949 moment frames under earthquake loading, J. Struct. Eng. 137 (2011) 1291–1302.
950 https://doi.org/10.1061/(ASCE)ST.1943-541X.0000376.
951 [52] F. Zareian, R.A. Medina, A practical method for proper modeling of structural damping in inelastic plane
952 structural systems, Comput. Struct. 88 (2010) 45–53. https://doi.org/10.1016/j.compstruc.2009.08.001.
953 [53] J.M. Castro, A.Y. Elghazouli, B.A. Izzuddin, Modelling of the panel zone in steel and composite moment frames,
954 Eng. Struct. 27 (2005) 129–144. https://doi.org/10.1016/j.engstruct.2004.09.008.
955 [54] T. Falborski, A.S. Hassan, A.M. Kanvinde, Column base fixity in steel moment frames: Observations from
956 instrumented buildings, J. Constr. Steel Res. 168 (2020) 105993. https://doi.org/10.1016/j.jcsr.2020.105993.
957 [55] G.A. MacRae, Y. Kimura, C. Roeder, Effect of Column Stiffness on Braced Frame Seismic Behavior, J. Struct.
958 Eng. 130 (2004) 381–391. https://doi.org/10.1061/(ASCE)0733-9445(2004)130:3(381).
959 [56] D.A. Foutch, S.Y. Yun, Modeling of steel moment frames for seismic loads, J. Constr. Steel Res. 58 (2002) 529–
960 564. https://doi.org/10.1016/S0143-974X(01)00078-5.
961 [57] J.M. Fisher, L.A. Kloiber, Base Plate and Anchor Rod Design, AISC Steel Des. Guid. 1. (2006) 73.
962 [58] A.M. Kanvinde, D.A. Grilli, F. Zareian, Rotational stiffness of exposed column base connections: Experiments
963 and analytical models, J. Struct. Eng. 138 (2012) 549–560. https://doi.org/10.1061/(ASCE)ST.1943-
964 541X.0000495.
965 [59] Federal Emergency Management Agency, Quantification of building seismic performance factors, FEMA P-695
966 ATC-63 Proj. (2009) 421.
967 [60] V. Silva, S. Akkar, J. Baker, P. Bazzurro, J.M. Castro, H. Crowley, M. Dolsek, C. Galasso, S. Lagomarsino, R.
968 Monteiro, D. Perrone, K. Pitilakis, D. Vamvatsikos, Current challenges and future trends in analytical fragility
969 and vulnerability modeling, Earthq. Spectra. 35 (2019) 1927–1952. https://doi.org/10.1193/042418EQS101O.
970 [61] Federal Emergency Management Agency, HAZUS-MH MR4 Technical Manual, Natl. Inst. Build. Sci. Fed.
971 Emerg. Manag. Agency (NIBS FEMA). (2003) 712.
972